Copper-doped ceria catalytic activity for soot oxidation process

Musakana, Fadzai Praise

Master's thesis / Diplomski rad

2022

Degree Grantor / Ustanova koja je dodijelila akademski / stručni stupanj: **University of Zagreb, Faculty of Chemical Engineering and Technology / Sveučilište u Zagrebu, Fakultet kemijskog inženjerstva i tehnologije**

Permanent link / Trajna poveznica: https://urn.nsk.hr/urn:nbn:hr:149:102746

UNIVERSITY OF ZAGREB
FACULTY OF CHEMICAL ENGINEERING AND TECHNOLOGY

Fadzai Praise Musakana

COPPER-DOPED CERIA CATALYTIC ACTIVITY FOR SOOT OXIDATION PROCESS

Master's Thesis

Zagreb, September 2022

UNIVERSITY OF ZAGREB

FACULTY OF CHEMICAL ENGINEERING AND TECHNOLOGY

FADZAI PRAISE MUSAKANA

COPPER-DOPED CERIA CATALYTIC ACTIVITY FOR SOOT OXIDATION PROCESS

Submitted in partial fulfilment of the requirements of the Master's in chemical engineering at the University of Zagreb

MASTER'S THESIS

Supervisor: Prof. dr. sc. Stanislav Kurajica

Co-supervisor: Dr. sc. Katarina Mužina

Zagreb, September 2022

ABSTRACT

Diesel engines in the automotive industry have optimal fuel efficiency, high durability, and low carbon dioxide emissions but carbonaceous soot formed during the combustion process is a major health and environmental concern. Catalytic converters are introduced to address this environmental issue. Catalytic soot oxidation is a method of reducing the emission of soot particles. Soot oxidation can be accomplished with a range of different catalysts. Most catalytic converters use mixed-metal oxides combined with noble metals as catalysts, which are extremely expensive. This study's main objective is to demonstrate that an alternative catalyst involving ceria oxide doped with a transition metal, in this case, copper, could achieve admissible results, reduce carbon footprint, and be a more cost-effective and sustainable substitute. The cerium oxide powders were obtained using combustion synthesis. Various cerium oxide catalyst samples were prepared, and their catalytic performance was evaluated. The materials' physicochemical properties were validated using XRD, SEM, FTIR, and TGA/DTG techniques. Cu-doped ceria nanocatalysts had smaller crystallite sizes and increased carbon oxidation activity. This study demonstrated how the use of copper doped ceria has the potential to effectively reduce harmful emissions less expensively and more sustainably.

Keywords: Copper doped ceria, catalyst, catalytic soot oxidation, nanocatalyst

ACKNOWLEDGEMENTS

I would like to express my deepest gratitude and thankfulness to the following people:

My supervisor, Prof. dr. sc. Stanislav Kurajica for his support, guidance, and patience throughout my studies. Thank you for providing me with the materials and laboratory facilities.

My co-supervisor, dr. sc. Katarina Mužina for her congenial personality, continuous patience, understanding, and sharing of knowledge. Thank you for providing me with your valuable time, and taking me step-by-step -through the processes, the materials, and laboratory facilities.

My father, Mr. F. Musakana for his continuous motivation, love, prayers, and support of my hopes and dreams and always being understanding as well as the financial support for my studies. I will forever be grateful. My siblings and best friends, Tanyaradzwa, Anotida, Hamidat, Danijella, and Ana, for always being there for me and pushing me to do better each time.

Ana Krpina and the Krpina family for being my support system through my deepest and loneliest time far away from home.

My colleagues in the faculty: Chekwube, Ivana, and Antoneta for their academic assistance and pleasant company during my studies.

The faculty and Dean of the faculty, for the pleasant opportunity to pursue my Master's degree and for providing funding in the first year of my studies.

I would like to dedicate this to my sweet and dear mother, Mrs. P. Musakana who began this journey with me but is now resting in peace. I love you. We will meet again.

Above all, I would like to give thanks to the almighty God for giving me strength and guidance to start and finish my Master's in Chemical engineering journey and for making all things possible.

Contents

LIST OF ABBREVIATIONS

DOC-Diesel oxidant catalyst

CRT- Continuously Regenerating trap

DPF- Diesel Particulate filter

SOF- Soluble Organic Fraction

PM- Particulate Matter

SCR- Selective Catalytic Reduction

CDPF- Catalytic Diesel Particulate Filter

TGA-Thermogravimetric Analysis

DTA- Differential Thermal Analysis

XRD- X-Ray Diffraction

SEM- Scanning Electron Microscope

TEM- Transmission Electron Microscopy

FTIR- Fourier -Transform Infrared Spectroscopy

HC- Hydrocarbon

ATD- After-treatment device

CI- Compression Ignition

CB- Carbon black

EGR-Exhaust gas recirculation

IF- Inorganic Fraction

PAHs- Polycyclic aromatic hydrocarbons

OSC- Oxygen Storage Capacity

KAS- Kissinger-Akahira-Sunose

1. CHAPTER 1

1.1 Introduction

Soot is described as a mass of impure carbon particles from the incomplete combustion of hydrocarbons. It is produced during the high-temperature pyrolysis or combustion of hydrocarbons; it is composed mostly of carbon; other elements such as hydrogen and oxygen are usually present in small amounts. It often contains a soluble organic fraction (SOF) whose constituents include aromatic compounds as well as various other unburned hydrocarbons [1]. It is universally accepted that soot formation steps can be summarized as (1) formation of molecular precursors of soot, (2) nucleation or inception of particles from heavy polycyclic aromatic hydrocarbon molecules, (3) mass growth of particles by addition of gas-phase molecules, (4) coagulation via reactive particle-particle collisions, (5) carbonization of particulate material, and, finally, (6) oxidation of polycyclic aromatic hydrocarbons and soot particles [1]. The competition between soot formation and oxidation determines the emission of soot from a diesel engine. The diesel engine combustion process produces soot which is known as a highly carbonaceous material that is an environmental pollutant. In comparison to gasoline engines, diesel engines emit less carbon dioxide, which makes them highly favourable. However, diesel engines are high emitters of particulate emissions: about 0.2–0.5 % of the fuel mass is emitted as small (~0.1μm diameter) particulates [1]. Human health is harmed by the suspension of this minute particulate matter (PM) in the atmosphere, which has both short- and long-term consequences. The need to control soot emissions due to environmental and health concerns, while also promoting the more efficient use of hydrocarbon fuels, necessitates the development of more economical and efficient diesel engines, which in turn requires the inclusion of catalysts to facilitate the soot oxidation process. Stringent measures have been taken into account to control vehicle emissions. Since 1992, European Union regulations have been imposed on new cars to improve air quality - meaning a car has to meet a certain Euro emissions standard when it is made [2]. Emission regulations will be further explained in the next Chapter. Current diesel engine emission control requirements have resulted in the widespread use of diesel particulate filters (DPFs), which efficiently collect soot particles from the exhaust and then oxidize them in a process known as regeneration. Direct oxidation of soot can be accelerated by incorporation of catalysts (typically transition and rare earth metals

oxides) in the DPF (a so-called catalytic DPF, CDPF) at typically a lower temperature than that required for pure thermal oxidation (>650 °C) [3]. In catalytic soot abatement, good contact between the catalyst and soot is required, therefore the morphology of the catalyst is an important characteristic of soot reduction. Rare earth-based catalysts are widely used in automotive exhaust purification catalysts, ceramics, rare earth polymers, fuel cells, coatings and many other fields because of their unique chemical and physical properties [4]. In this study, the effect of copper doping on ceria as a catalyst for soot oxidation was thoroughly investigated. The characteristics of the catalyst were evaluated using X-ray diffraction (XRD), scanning electron microscopy (SEM), and Fourier-transformed infra-red spectroscopy (FTIR) while soot oxidation catalytic performance was investigated using thermogravimetric analysis (TGA).

1.2 Diesel Vehicle Emission

To understand what diesel emissions are, an understanding of how a diesel engine operates needs to be established. The concept behind how it works is by compressing only air, or air with a combination of residual combustion gases from the exhaust (known as exhaust gas recirculation (EGR)). During the intake stroke, air is inducted into the chamber, and compressed during the compression stroke. This allows the air temperature inside the cylinder to increase to a high degree such that diesel fuel injected into the combustion chamber ignites. This creates a heterogenous air-fuel mixture in which the dispersion of the fuel is uneven due to the fuel being injected into the air just before combustion. The torque that diesel engine produces is controlled by manipulating the air-fuel ratio (λ); instead of throttling the intake air, the diesel engine relies on altering the amount of fuel that is injected, and the air-fuel ratio is usually high [5]. Due to its very high expansion ratio and inherent lean burn which enables heat dissipation by the excess air, the diesel engine has the highest thermal efficiency (engine efficiency) of any practical internal-combustion engine [5]. It has a theoretical efficiency of 75% [6]. Low-speed diesel engines (as used in ships and other applications where overall engine weight is relatively unimportant) can reach effective efficiencies of up to 55% [7]. In summary the diesel engine operates on the following principles: compression ignition, heterogeneous air-fuel mixture, high air ratio, diffusion flame, torque adjustment solely by

mixture quality, fuel with high ignition performance (cetane rating) ,and mixture formation inside the combustion chamber.

1.2.1 Diesel vehicle emission

Emissions from diesel engines are extremely complex mixtures. The composition of diesel exhaust differs depending on engine type and operating conditions, fuel, lubricating oil, and the presence or absence of an emissions control system. Diesel produces many harmful emissions when it is burned. Therefore, diesel engines are considered as one of the largest contributors to environmental pollution caused by exhaust emissions, and they are responsible for several health problems as well. Diesel emissions consist of a wide range of pollutants that are toxic at high concentrations. These include organic and inorganic compounds dispersed among the gaseous and particulate phases: CO, CO_2, NO, NO_2, N_2O, NH_3, Volatile organic compounds and water vapor, Hydrocarbons (HC), Polynuclear aromatic hydrocarbons, Carboxyl compounds, Organic acids, halogenated organic compounds, Sulfur dioxide, and Dioxins. Figure 1 shows the approximate composition of diesel exhaust gas [8]. As shown in Figure 1, the four main pollutant emissions from diesel engines are carbon monoxide-CO, hydrocarbons-HC, particulate matter-PM, and nitrogen oxides-NOx.

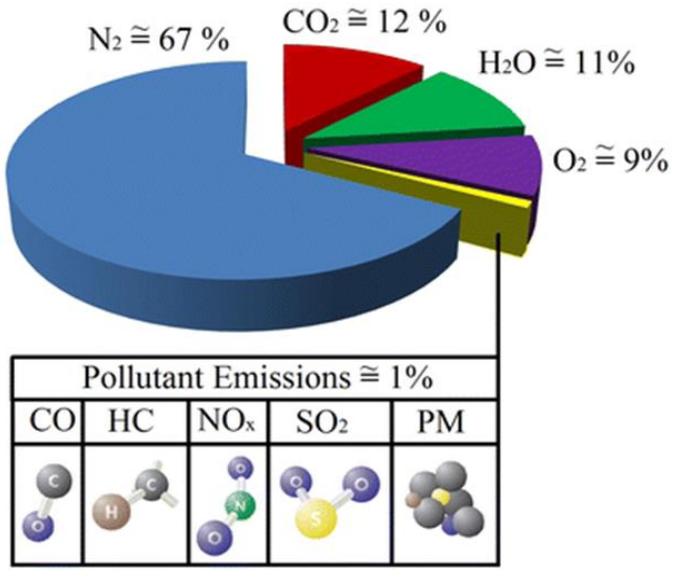

Figure. 1 The compositions of diesel exhaust gas [8]

1.2.2 Diesel Particulate Matter

The term particulate matter (PM) can be used to refer to a complex mixture of organic and inorganic solids, liquids, powders, and droplets suspended in the air which includes fine dust, soot, mist, fog, and smog [9]. In the narrower context of vehicle emissions, this can be considered all substances, other than unbound water, which are present in exhaust gas in the solid or liquid phases [10]. In both diesel and gasoline engines, soot particulates form because of incomplete or partial combustion of fuel. This can happen because of elevated temperatures and local sub-stoichiometric oxygen conditions, which prevent complete combustion to CO_2. This has historically been an issue for diesel vehicles as their compression ignition (CI) engines inject fuel directly into the combustion chamber, preventing sufficient air/fuel mixing on a molecular level and resulting in localised fuel-rich regions which do not undergo full combustion [10]. Increasing the engine load or its capacity to produce power has been reported to decrease diesel PM emissions (per kilometre) due to greater efficiency of combustion, as well as reducing the metal content [11]. Ambient temperature is also a factor in the quantity of particulate emissions, as low temperatures during ignition (known as "cold start") decreases the air-fuel ratio, lowering oxidation and increasing carbon formation [12]. Figure 2 shows some size definitions for atmospheric particles. PM10 particles are particles with a diameter of less than 10 μm that can pass through mucus and cilia in the nose and throat when inhaled. Particles in the "nucleation" mode primarily consist of condensed volatile materials and have a particle size typically below 30 nm. While the "accumulation" mode consists of the larger carbonaceous particles typically greater than 100-300 nm in size. The World Health Organisation (WHO) considers that fine particles (PM2.5) are "strongly associated with mortality and other endpoints such as hospitalization for cardio-pulmonary disease", but that no specific size threshold could be identified below which no adverse health effects occurred. It also considers the extractable organic compounds of particulate matter (especially PAHs) to "exert pro-inflammatory as well as adjuvant effects" [9].

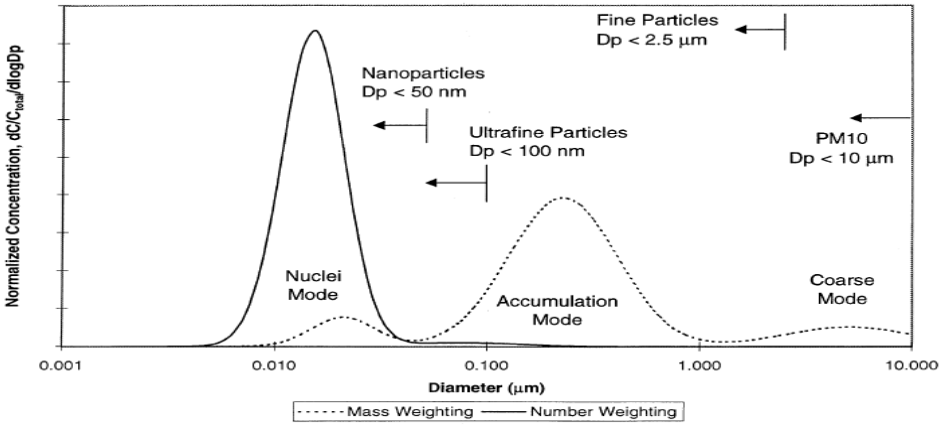

Figure 2. Typical size distribution of particulate matter from diesel exhaust by mass and number [12]

1.3 Diesel Emission Regulations

The World Health Organization estimated that around 2.4 million people die every year due to air pollution (WHO 2007) [8]. In today's world, environmental protection, climate change, and air pollution have become subjects of central concern. Many established agencies, organizations (EPA, OECD, IPCC, IEA, EEA, etc.) worldwide have been working to prevent air pollution and climate change caused by pollutant emissions. In their works, they have reported that approximately the 20–30 % of pollutant emissions originate from transport and these emissions have an important impact upon global warming and climate change [8]. To prevent the effects of these pollutant emissions, they have emphasized on such issues as making several legal arrangements, advancing the technological developments, creating several model structures, developing control systems, and organizing the structure of traffic (OECD 2011; EPA 2012; IEA 2012; IPCC 2007; OECD 2002; EEA 2012) [8]. Diesel engines have extensive usage compared to gasoline engines because of their low-operating costs, energy efficiency, high durability, and reliability. However, their major concern is diesel exhaust gas contains higher amount of particulate matter and NOx emissions which contribute tremendously to environmental and health problems. According to health experts, pollutants emitted by diesel engines are harmful to human health, cause air, water and soil pollution cause acid rain, ground-level ozone, and reduce visibility. NOx emissions in particular contribute to acidification, formation of ozone, nutrient enrichment, and smog formation, which have become extensive problems in most key cities worldwide. As mentioned previously, European Union regulations are imposed on vehicles such that new models have to meet a certain Euro emission standard during their construction. Table 1 shows Euro standards for M1 and M2, N1 and N2 vehicles

as defined in Directive 70/156/EC with reference mass B2,610 kg [2]. In this table, the limits are defined in mass per energy (g/kWh) Although emissions regulations have been in place since 1970, the first EU-wide standard, known as Euro 1, was not implemented until 1992. Catalytic converters became mandatory on new cars under Euro 1, effectively standardizing fuel injection. Since then, a series of Euro emissions standards have been introduced, culminating in the current Euro 6, which was introduced in September 2014 for new type approvals. Control emission systems must be used in addition to these standards to prevent emissions. Additional regulations concerning the sulfur level in fuel were applied by European legislations. Since sulfur may inhibit catalyst activity, lowering the fuel sulfur level is of benefit to both the particulate emissions and the implementation of certain aftertreatment technologies. Before 2005 the permitted fuel sulfur level was 350ppm, but it was lowered in Europe to 50ppm by 2005.

The pollutant emissions from diesel- engine vehicles in (g/Kwh)

Table 1 Euro standards for European Union for heavy-duty vehicles (Delphi et al. 2012)

	CO	HC	NOX	PM
Euro I	4.5	1.1	8.0	0.61
Euro II	4	1.1	7.0	0.15
Euro III	2.1	0.66	5.0	0.13
Euro IV	1.5	0.46	3.5	0.02
Euro V	1.5	0.46	2.0	0.02
Euro VI	1.5	0.13	0.4	0.01

1.4 Soot

Soot formation

Diesel particle emissions can be divided into three main components: soot, soluble organic fraction (SOF), and inorganic fraction (IF). More than 50 % of the total PM emissions are soot that is seen as black smoke [8]. Because the particulates are primarily composed of a carbonaceous fraction containing elemental and organic carbon, they are commonly referred

to as "soot." Aforementioned soot is formed when pyrolysis of the fuel molecules occurs forming small unsaturated molecules, usually ethyne due to lack of oxygen. These molecules undergo polymerisation as shown in Figure.3 followed by ring closure to form polycyclic structures. The next phase is nucleation, in which these graphite-like structures stack to form “crystallites,” which in turn stack in a random orientation around the centre of the particle to form “turbostratic particles” [13]. Coagulation and surface growth then takes place which is instigated by the addition of gaseous carbonaceous species [10]. Surface growth slows as the temperature drops, and "primary soot particles" form. These continue to coagulate to form chainlike aggregates that can themselves accumulate to from large agglomerates [10]. As the temperature drops, various volatile or soluble organic compounds (known as the soluble organic fraction, SOF) condense and can form small particulates or be adsorbed onto the surface of existing soot particles. The SOF is comprised of polycyclic aromatic compounds that contain oxygen, nitrogen, and sulphur, all of which are produced during the combustion of the fuel. Some of the sulphur in the fuel is oxidized to SO_3, which can result in the formation of sulphuric acid and sulphates on the particles.

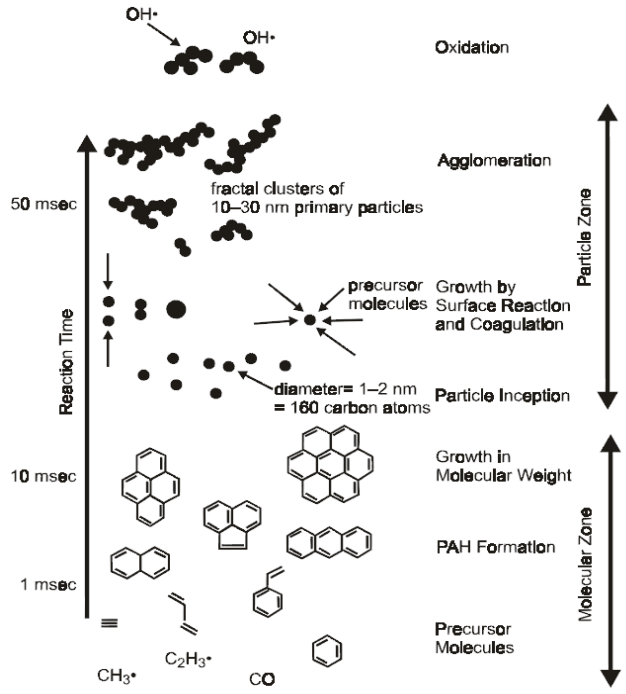

Figure 3. Schematic mechanism of the formation of soot particles [14]

CHAPTER 2

2.1 Diesel Particulate Filter

DPFs have been used in vehicle production since 2000. They are generally made of cordierite ($2MgO–2Al_2O_3–5SiO_2$) or silicon carbide (SiC) honeycomb structure monolith with the channels obstructed at alternate ends to remove PM emissions from exhaust gas. The plugged channels at each end force the diesel particulates matters through the porous substrate walls, which act as a mechanical filter (Fig. 4) [8] Cordierite is a synthetic ceramic developed for flow-through catalyst substrates and subsequently adapted for the filter application [15]. For a long time, silicon carbide has been used in a various industry for applications such as semiconductors, abrasives, and elevated temperature/molten metal contact materials. Cordierite substrates perform satisfactorily in most heavy-duty applications with high exhaust temperatures. Cordierite, on the other hand, is more susceptible to thermal stress-related damage in low-temperature operation, which may induce "uncontrolled regenerations." In high thermal stress applications, silicon carbide has higher maximum operating temperature limits and greater durability. Diesel particulate filters (DPF) capture soot particles and prevent them from entering the exhaust system. Soot particles are transported into the pore walls by diffusion as they pass through the walls. This filter has a lot of parallel channels most of which are square. The thickness of the channel walls is typically 300–400μm [8]. Channel size is specified by their cell density (Typical value: 100–300 cpsi) [8]. Wall flow ceramic monoliths, which are derived from the flow-through cellular supports used for catalytic converters, became the most common type of diesel filter substrate (originally reported by Howitt and Montierth [15]). The primary benefit of the wall flow particulate filter is the high surface area per unit volume, which, when combined with the high collection efficiencies (over 95 percent), makes this technique very appealing. The filter walls are designed with an optimal porosity, allowing exhaust gases to pass through without much resistance while remaining impervious enough to collect particulate species. A layer of soot forms on the surface of the channel walls as the filter becomes increasingly saturated with soot. This results in highly efficient surface filtration for the subsequent operating phase. However, oversaturation must be avoided. As the filters accumulate PM, backpressure builds up, which has a variety of negative consequences, including increased fuel consumption, engine failure, and filter stress. To avoid these negative consequences, the DPF must be regenerated by burning trapped PM.

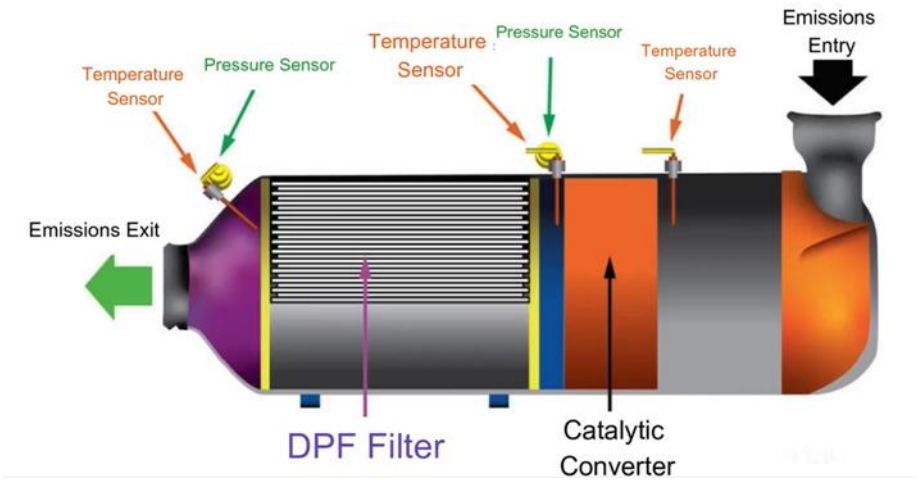

Figure 4. DPF system diagram [16]

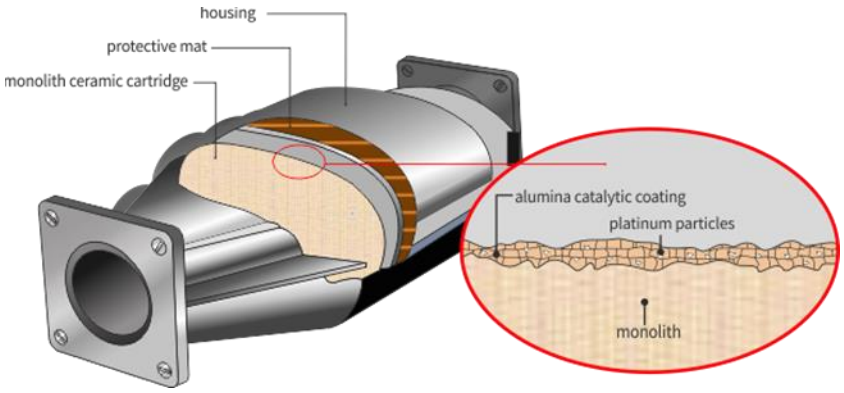

Figure 5. DPF structure [17]

According to Figure 5 the walls of the filter cartridge (monolith) have a structure of small size pores, which are carefully controlled in the production process. The total porosity of the material is usually between 45 and 50% or more, while the average pore sizes are typically between 10 and 20 μm. In monolithic wall filters, the filtration mechanism is a combination of wall penetration and soot cake. In the first place, wall penetration is the dominant filtration mechanism because solid particles are deposited in the pore network within the wall material. As the soot charge increases, a layer of particles forms along the inlet channel wall surface, and soot cake filtration takes over as the dominant mechanism. Monolithic filters typically have a filtration efficiency of 70 to 95 percent of all solid particles. In order to provide a substrate for catalytic (noble) metals and physically separate and prevent undesirable reactions between components of the complex catalytic system, catalytic coating is applied to a monolith with a water-based suspension. Catalytic coating materials include inorganic non-noble metal oxides such as alumina, silicon oxide, cerium oxide, titanium dioxide, zirconium oxide, and zeolites. DOC, DPF, and SCR are examples of diesel exhaust after treatment systems. Although

regeneration is a major issue for DPFs, many studies and research have been conducted in recent years to address this issue and reduce soot oxidation temperatures. These after-treatment systems are the most popular, particularly for heavy-duty diesel engines, and a combination of DOC, DPF, and SCR is typically used for the simultaneous removal of major pollutant emissions from diesel engine exhaust. DPFs are commonly used in conjunction with DOC to eliminate PM emissions from diesel exhaust gas. The aforementioned after-treatment systems are typically made of cordierite SiC. This structure functions as a mechanical filter, removing 100% of the PM emissions from diesel exhaust gas [18].

2.2 DPF Regeneration

Active regeneration

There are subsequently two types of regeneration processes of DPFs which will be looked at in this study, which are, active regeneration and passive regeneration. In an active regeneration of DPF, PM is oxidized periodically by heat supplied from external sources, such as an electric heater or a flame-based burner. Active regeneration is periodically applied to DPFs in which trapped soot is removed through a controlled oxidation with O_2 at 550℃ or higher temperatures [18]. The exhaust gas temperature could reach 800℃. In this case, active regeneration occurs when the engine isn't producing enough heat, for example in a truck that isn't fully loaded. When the amount of soot in the exhaust reaches a certain threshold, the engine injects fuel into the exhaust stream, which passes over the oxidation catalyst and oxidizes the fuel to generate heat. The heat produced by fuel oxidation is then used to convert soot to carbon dioxide. Similar to passive regeneration, active regeneration can occur automatically any time the vehicle is in motion. The burning of PMs, captured in the filter, takes place as soon as the soot loading in the filter reaches a set limit (about 45 %) indicated by pressure drop across the DPF [18]. Active regeneration faces considerable challenges due to the higher regeneration temperature and a large amount of energy required for heat supply. While temperatures as high as the melting point of the filter cause DPF failure, the need for energy for heating increases the system's production cost due to complex supplements. These negative effects regard active regeneration as undesirable.

Passive regeneration

The entire process of passive regeneration is very simple, quiet, effective, and fuel efficient, which means that neither the vehicle operator nor the vehicle's engine management system must do anything to induce DPF regeneration. The passive regeneration method, also known as the continuously regenerating trap (CRT) system, is characterized by diesel oxidant catalyst (DOC)-assisted DPF regeneration. In this process, a wall flow silicon carbide filter is used in conjunction with DOC, a sophisticated engine management system, and sensors. NO_2 provides a more effective oxidant than oxygen and so provides optimum passive regeneration efficiency [8]. The CRT system is installed with a DOC where NO is preferentially converted to NO_2 before a DPF and NO_2 is used to oxidize PM trapped in the filter below 300 °C [18]. Thus, the burning temperature of PMs is reduced whilst the NO_2 to NO ratio is increased. To achieve the best performance, however, the CRT system should satisfy two conditions: the temperature should be in the range 250–450 °C and the NO_x/soot ratio should be adequately high [18]. Otherwise, the NO_2 produced will be insufficient to oxidize soot. It should be noted that both hydrocarbons (HC) and carbon monoxide (CO) would be secondary pollutants caused by incomplete oxidation conversion of soot in the CRT system. Since the regeneration occurs at high exhaust temperatures, DOC must be used upstream a wall flow SiC filter, which is the most widely used DPF filters in the world. This obligation can be avoided by using catalysed DPFs (CDPF) that house the DOC formulation on the DPF itself. There is no DOC or aftertreatment system upstream of the DPF in this system, and all reactions occur in the CDPF. When compared to a wall flow SiC filter, CDPF with Pt as a catalyst has the same conversion efficiency. The oxidation temperature of soot can be reduced using CDPFs. In addition to the oxidation occurring in DPF may be realized at lower temperatures, the conversion rate can be further increased using biodiesel or fuel additives [8]. Passive regeneration occurs when the exhaust temperature is high on the highway. The exhaust first passes through the diesel oxidation catalyst (DOC), followed by the diesel particulate filter, which captures soot particles within the aftertreatment device (ATD). Passive regeneration occurs when the engine temperature rises to the point where soot, or carbon, reacts with oxygen to form carbon dioxide. Since carbon dioxide is a gas, it can pass through the filter.

Unlike in the active regeneration, in passive regeneration of DPF, the oxidation of PMs occurs at the exhaust gas temperature by catalytic combustion promoted by depositing suitable

catalysts within the trap itself [18]. In this case, PM is oxidized by an ongoing catalytic reaction process that uses no additional fuel. Under a temperature range between 200 and 450 °C, small amounts of NO_2 will promote the continuous oxidation of the deposited carbon particles [18]. This is the basis of the continuously regenerating trap (CRT) which uses NO_2 continuously to oxide soot within relatively low temperatures over a DPF [18]. Due to the low bulk density of diesel particulates, which is typically below 0.1 g/cm^3 (the density depends on the degree of compactness; as an example, a number of 0.056 g/cm^3 was reported by Wade [19], diesel particulate filters can quickly accumulate considerable volumes of soot [19]. Thermal regeneration of diesel particulate filters is typically employed, where the collected particulates are oxidized—by oxygen and/or nitrogen dioxide—to gaseous products, primarily to carbon dioxide [19]. Thermal regeneration, schematically represented in Figure 6, is undoubtedly the cleanest and most attractive method of operating diesel particulate filters.

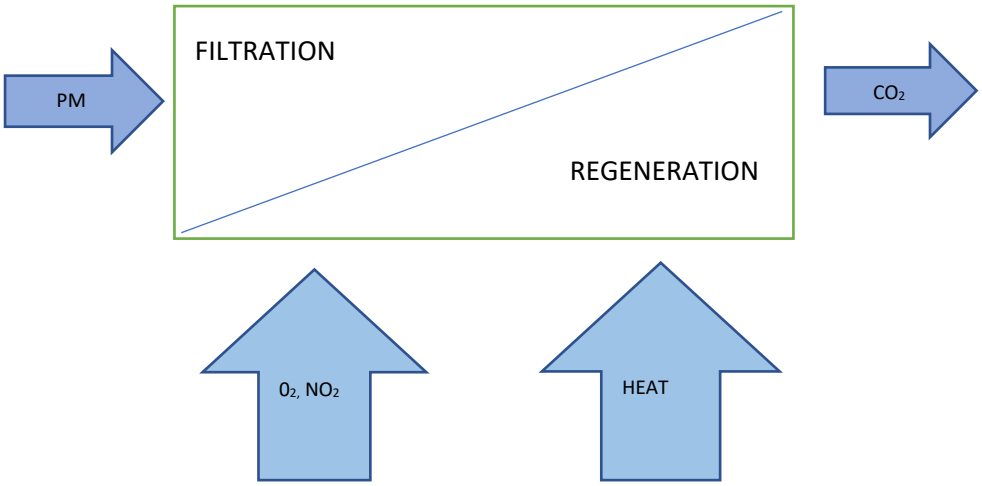

Figure 6. The concept of particulate filter with thermal regeneration

2.3 Soot Oxidation

General

The TGA analysis of the soot samples improved our understanding of the kinetic behavior and parameters of real soot**.** Beside carbon, soot particles are composed of polycyclic aromatic hydrocarbons (PAHs), which have either planar or curved structures [20]. The oxidation behaviours of soot particles vary depending on their structure, PAH arrangement, and surface functional groups. The oxidation rate of curved PAHs in soot is thought to be higher than that of planar ones [20]. Soot particles and polycyclic aromatic hydrocarbons (PAHs) are produced by incomplete combustion of hydrocarbons and are commonly found in engine and furnace emissions. In engines, poor fuel-air mixing creates fuel-rich zones that promote soot formation at elevated temperatures. Soot particles are the second largest contributor to global warming (after CO_2) and participate in increasing regional temperatures and accelerating the melting of polar [20]. To meet stringent air quality standards, it is therefore critical to reduce the formation or, at the very least, the emission of soot and PAHs into the environment by oxidizing them. Particulate filters are used in engine exhaust pipelines to capture soot particles and reduce their emission to the environment. Soot oxidation in a diesel particle filter is affected by many factors, such as (i) the composition, flow rate, and temperature of the exhaust gas, (ii) the physical, chemical, and structural properties of soot, and (iii) the trap characteristics (shape, material, type, and concentration. of catalysts. There are two possible reactions in the DPF. The first is NO_2-assisted soot oxidation, and the second is classical soot oxidation, also known as the active oxygen mechanism.

Uncatalyzed soot oxidation

A number of factors affect the reactivity of carbon materials, these include crystallite size/orientation, the concentration of structural defects, and the location, type, and concentration of impurities. These properties control the “active surface area” which is the fraction of a carbon material susceptible to oxygen-carbon reactions [13]. Moulijn et al. conducted several studies on the carbon-oxygen reaction and proposed a stepwise mechanism that included simplified oxygen complexes and graphitic carbon structures, as shown in Figure 7 [13].

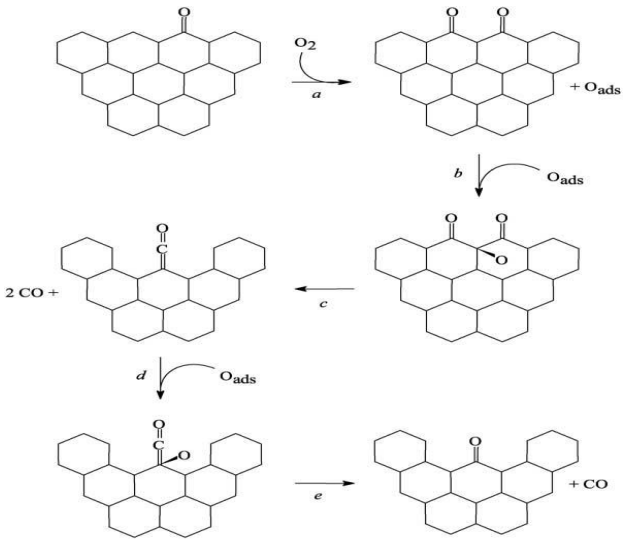

Figure 7. Reaction mechanism of uncatalyzed oxidation of carbon [13]

Step a) A surface semiquinone group and physically adsorbed oxygen are formed when graphite with a ketone "surface-oxygen complex" (SOC) reacts with gas phase O_2. Because the semiquinone complex's C-C bond strength is only slightly weaker than that of graphite, it is unlikely to decompose and is thus a "stable surface-oxygen complex."

b) Because of the electronegativity of the oxygen atoms in the semiquinone complex, the C atom between the CO groups becomes a target for oxygen bonding. A semiquinone complex with off-plane oxygen is formed, which lessens the C-C bond strength of the neighbouring C atoms.

c) Since the C-C bonds of the neighbouring carbon atoms are weakened, the complex decomposes to CO, leaving a graphite structure with a carbonyl group.

d) Due to the electronegativity of the oxygen in the carbonyl group, the carbon atom next to it becomes a target for bonding with oxygen. A carbonyl group is formed with off-plane oxygen.

e) Consequently, the C-C bond strength in the neighbouring carbon atom reduces, which decomposes to release CO, leaving another structure with a SOC, and the reaction cycle can then start again with step a).

Notably, the reaction rate in the steady state is determined by the number of carbon complexes on the active surface area rather than the rate-constants of the individual steps.

Catalysed soot oxidation

Generally, the process of catalytic soot oxidation is slow, because the solid particles are large and, when deposited, immobile. For this reason, they do not penetrate into the catalyst's micropores or mesopores where catalytic processes normally occur. Rather, soot oxidation occurs on the filter walls of the particle filter where the catalyst has been deposited. Soot oxidation can be accomplished through direct or indirect contact with a catalyst. Indirect contact catalysis does not require direct physical contact between soot and catalyst. Instead, they act by catalysing the formation of a mobile compound that is more reactive than O_2 (e.g., NO_2, O_{ads}, etc.) [13]. Generally, catalytic soot oxidation in laboratory conditions is investigated using two approaches of soot/catalyst contact, direct and indirect contact also referred to as tight or loose contact:

Direct and Indirect contact soot oxidation

Achieving direct contact soot oxidation under real-world scenarios is challenging due to the difficulty in establishing intimate contact between catalyst and soot on a particulate filter [13]. Several studies have shown the importance the degree of contact with soot has on the activity achieved by a catalyst [21, 22]. The investigations by Neeft et al. [22] into catalyst/soot contact established the definition of two types of contact; "loose" – which involves mixing of the catalyst and soot with a spatula, and "tight" – whereby intimate contact between catalyst and soot is achieved by mechanical grinding [23]. They discovered that the soot oxidation temperatures under tight contact were considerably lower than those under loose contact with each of the metal oxide catalysts tested, with differences of up to 200 ºC. Comparisons between the soot oxidation temperatures achieved by catalysts from different studies should be approached with caution due to the difficulties in establishing comparable testing conditions [24]. In this study, tight contact was established using mortar and pestle to mix the contents. In direct contact, the catalyst can either activate the carbon atoms or act as a renewable, activated oxygen donor [13]. There are two main reaction mechanisms for indirect contact catalysts, one being the "NOx-aided gas-phase mechanism" which catalyses the oxidation of NO to NO_2 in order to accelerate soot combustion [25].

$2NO + O_2 \longrightarrow 2NO_2$

$NO_2 + C \longrightarrow NO + CO$

$N0_2 + CO \longrightarrow NO + CO_2$

CHAPTER 3

3.1 Ceria

General

More than 90% of chemical manufacturing processes involve catalysis [26, 27]. Catalysts increase the rate of a chemical reaction by lowering the activation energy barrier. Catalysts provide alternative reaction paths that are less energetic and have higher selectivity by facilitating the cleavage and formation of chemical bonds in reactant and product molecules. Heterogeneous catalysis is a surface phenomenon by which one or more reagents adsorb reversibly on a surface – typically a supported transition metal – on which subsequent reactions occur [28]. By reducing at least one dimension of a catalytic particle to the nano scale (1-100 nm) several advantages are gained; surface to volume ratio increases and number of atoms exposed at the surface increases – this more efficiently utilizes potentially expensive metals [28]. Furthermore, the band gap, intrinsic reactivity, and catalytic potential are modified. By tailoring catalyst particle size and shape, surface reactivity at the nanoscale can be manipulated [29].

3.1.1 Ceria (Cerium oxide)

Ceria-based oxides have grown in importance as active advanced materials and co-catalysts in energy conversion systems and applications of environmental sustainability. Development of advanced ceria-based catalysts is an ongoing research topic for applications in car exhaust gas pollution control, fuel cells, photocatalysts and chemical processes. This study also focuses on ceria nanostructures and doped ceria, characterization, and catalytic applications of ceria-containing catalysts. Cerium belongs to the group of lanthanides in the periodic system of elements, which are a section of the so-called rare earth elements. It is the most abundant among the rare-earth elements, and it is more abundant than nickel or copper. In nature, cerium can be found in various minerals such as monazite, loparite, and bonazite. By different extraction procedures, most commonly liquid -liquid extraction, selective precipitation or ion exchange

processes, cerium is commercially obtained as oxalate, carbonate, or hydroxide precursor [30]. Calcination easily converts these cerium precursors to cerium dioxide, also known as ceria. Elemental cerium has an electronic configuration of $[Xe]4f^{1}5d^{1}6s^{2}$ and can form both Ce^{4+} and Ce^{3+} oxidation states. Ceria gained particular attention as a catalyst and active species support in catalysis due to its ability to switch reversibly between Ce^{4+} and Ce^{3+} under repetitive redox cycles while attaining stability in the fluorite lattice (CeO_{2-x}, x=0-0.5) [31]. This redox switch and structure stability are unique to ceria and serve as the foundation for an important property of ceria used in catalysis, the so-called Oxygen Storage Capacity (OSC).The Ce^{4+} oxidation state is considered more stable than Ce^{3+} because its electronic structure is more stable (Ce^{4+} have electronic structure $[Xe]4f^{0}$ and Ce^{3+} $[Xe]4f^{1}$)[30]. Cerium exhibits a complicated phase diagram with two oxides namely cerium dioxide (CeO_2) and cerium sesquioxide (Ce_2O_3), but generally, cerium oxide is considered as CeO_2 because of its higher stability than Ce_2O_3.

Crystal structure

Ceria has a fluorite structure (FCC) with an Fm-3m space group. Figure 8 shows ceria consisting of a simple cubic oxygen sub-lattice with cerium ions occupying the cube centres. The structure of ceria has eight coordinated cerium and four coordinated oxygen, which means O anions are bonded to four Ce neighbours and Ce cations are bonded to eight O neighbours. Cerium is at the centre of tetrahedron with corners filled with oxygen atoms [32]. The cubic unit cell's lattice constant is 0.541 nm [33]. In ceria surface chemistry, crystal defects of ceria play a pivotal role. Notably, primary atomic defects include vacant lattice sites, interstitials, and foreign atoms. Foreign atoms may be present interstitially or substitutionary.

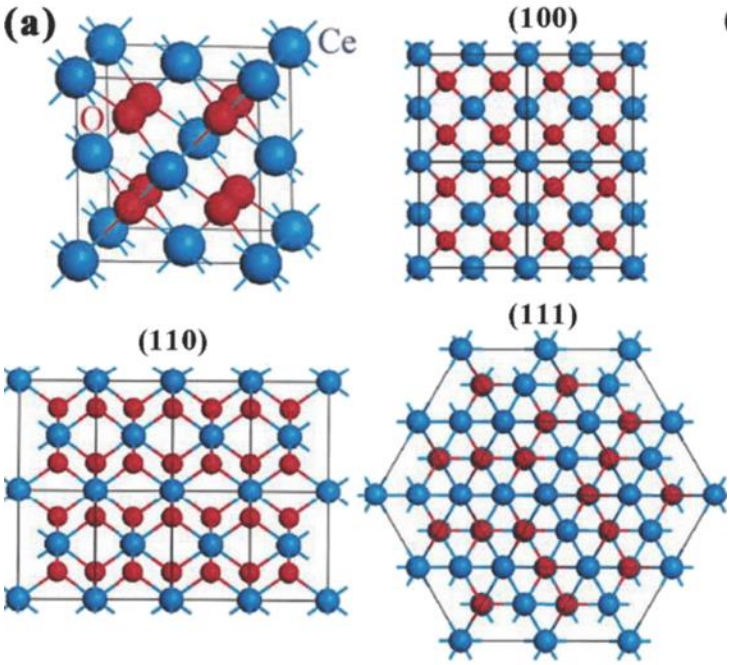

Figure 8. a) Face-centred crystal cell of the ceria structure with (100), (110) and (111) planes of the ceria structure [34].

3.1.2 Oxygen vacancies

The characteristic feature of storing and releasing oxygen reversibly has first been reported by Gandhi et al. [35]. As mentioned before, the reversible uptake of oxygen is based on a redox switch between Ce^{4+} and Ce^{3+}, which implies that under oxygen-deficient conditions oxygen is released from the ceria lattice to oxidize adsorbed compounds such as hydrocarbons, hydrogen, carbon monoxide or soot in the case of exhaust emission control [30]. Ceria is then present CeO_{2-x} form (with $x \leq 0.5$) which depends on the degree of oxygen removal. A high degree of oxygen removal correlates with an elevated level of oxygen vacancy formation. By substituting lower valent elements from the cation sub-lattice, cerium oxide can have a high oxygen deficiency. High oxygen ion conductivities are expected because of this property, asserting its potential applications as a solid electrolyte. In addition, for transport and carrier properties, the concentration of oxygen vacancies in the solid can play a significant role in oxygen-ion transport. As previously mentioned, three index lattice planes ((100), (110) and (111)) exist on the surface of ceria nanocrystals. The stability order of the planes is (111) > (110) > (100) and the activity is in the reverse order [34]. The degree of the oxygen mobility in the ceria lattice is related to the size, type, dispersion, and abundance of oxygen (anion) vacancies. Lower valence dopants can also be used to manipulate the oxygen vacancy content in the ceria lattice.

3.2 Nano ceria

Ceria nanoparticles generally comprise octahedral shapes and mainly most stable (111) facets are exposed in order to keep surface energy as small as possible. Nano cubes and nanorods have more oxygen vacancies on the surfaces because they can expose (100) planes. Meanwhile, other external or internal factors such as doping elements and temperature can affect the concentration of oxygen vacancies [36]. The reduction of particle size to the nanometre scale is in most cases associated with an apparent change of the physical and chemical properties as compared to bulk materials which translates to a different catalytic behaviour. Thus, tailoring ceria nanostructured materials with defined size and morphology leads to higher efficiency as compared to the bulk analogue. Furthermore, compared to bulk, nanoscale ceria shows phenomenal catalytic activity in many applications, which is associated with an increased specific surface area and facilitation of oxygen vacancy formation than that of the bulk material. The reactivity of ceria nanoparticles can be controlled by controlling their size so they can have improved size lattice relaxation, electronic conductivity, and other effects compared to bulk ceria. Cerium oxide nanoparticles have received more attention than other metal nanoparticles due to their unique properties; they can be used in chemical polishing/polarization, corrosion protection, fuel oxidation catalysts, sensors, solar cells, sunscreens, wound healing, anti-cancer applications, antibiotics, and drug delivery [37, 38].

3.3 Doped Ceria

When exposed to elevated temperatures, ceria loses specific surface area, resulting in a decrease in catalytic activity as well as deactivation of ceria in terms of oxygen storage capacity, especially at temperatures above 1123 K. This loss of surface area and OSC is based on effects of sintering in primary particles. To stabilize ceria thermally against sintering, it can be doped with different ions [24]. In this study copper doped ceria will be investigated as a catalyst in soot oxidation process. Recent studies have shown that CuO-CeO_2 catalysts could replace the noble metals for CO oxidation in the future because of their high activity and low-cost [39]. Copper doping favours an increase in the surface area of the copper-doped ceria catalysts and the formation of oxygen vacancies, thereby improving the redox properties [40]. The introduction of a lower oxidation number element into the crystal structure of CeO_2

nanoparticles aids the removal of some atoms in order to remain electroneutrality of the structure. This deficiency increases the system's entropy due to thermodynamic laws because formation of defects increases enthalpy. Taking Gibbs' free energy into account, up to a certain concentration, there is an enhancement of the stability of the crystal structure of cerium oxide. Doping cerium oxide nanostructures thus improves their chemical and thermal stability, ionic conductivity, and UV absorption. In the study, it is observed that copper doped ceria samples exhibit higher catalytic performance compared to bare CeO_2 and CuO catalysts. The numerous reports of doping of various metals such as Co, Mg, Cd, Fe, Ni, Ag, and Zn with CeO_2 nanoparticles have been presented that are associated with improving the properties of new nanostructures [38].

3.4 Investigations of CeO2 and doped Ce02 catalytic activity in soot oxidation process

Catalysis is the primary emerging application of applied CeO_2 materials. The interconvertibility of CeO_x materials is the core principle for the use of ceria as an oxidation catalyst. Cerium dioxide as a modifying additive within the $ZnO–CuO–CeO_2/Al_2O_3$/cordierite catalysts is shown to stabilize their operation. Optical and structural characterizations of doped ceria nano particles are performed to calculate the direct allowed bandgap, emitted fluorescent intensity, particle size, and lattice parameter as functions of dopant element and concentration. The average diameter of the nanoparticles can be calculated using Scherrer's formula from the full width at half maxima of and angular position of the XRD peak, usually (111) which corresponds to the most stable surface plane among the low-index planes of ceria (Deshpande et al. 2005) [41].

CHAPTER 4

4.1 Kinetics

Kinetic parameters are crucial for modelling diesel filter regeneration and designing more efficient regeneration techniques. Calculation of kinetic parameters from the TGA curves is based on the formal kinetic equation [43].

$$-\frac{dm}{dt} = k(T)f(m) \qquad (1)$$

where:

m: the actual mass of sample undergoing reaction

t: time

k: rate constant

T: absolute temperature

The kinetic characterization is occasionally based on iso-conversional methods which are mainly used for obtaining and evaluating the activation energy as a function of the degree of conversion [42]. Because thermographs and TGA results have partially superimposed peaks, mathematical models are commonly used to deconvolve them. It has been proven that the values obtained depend not only on factors such as atmosphere, gas flow, sample mass and heating rate, but also could depend on the mathematical treatment of the data [42]. Thermogravimetric analysis (TGA) used to determine the kinetics of composites degradation, gives integral curves that show dependence of mass loss on temperature. The soot sample is oxidized inside a furnace at a fixed or increasing temperature in the TGA, while its weight loss is continuously recorded. This test can determine both the typical oxidation temperatures and the kinetic parameters. When diesel soot is studied with TGA, both isothermal and non-isothermal tests are proposed and compared in the literature [43, 44]. In this study we will consider non isothermal conditions. Two disadvantages, however, are associated with the use of the TGA for characterization of the soot oxidation reaction. These are namely, dependency of the kinetic parameters upon the experimental conditions selected in the instrument (such as the gas flow rate, the heating ramp, or the initial sample mass) followed by, under specific operating conditions, the soot oxidation inside the TGA furnace could be a partially diffusion-controlled reaction. In this situation, the kinetic parameters cannot be deduced directly from the TGA curves, and a combination of kinetic models is necessary.

4.2 Kinetics in non-isothermal conditions

As mentioned before, (TGA/DTG) analysis method was applied to measure the weight changes and rates of weight loss used for calculating the kinetic parameters. Applying kinetic models

to the in-situ degradation reaction aids in the determination of the kinetics of the thermal behaviour of the soot sample. The reaction rate for non-isothermal experiments depends on both f (α) and k (T). Two ways are used in defining a non-isothermal method, differential and integral. The differential form of non-isothermal is expressed as follows [45]:

$$\frac{dx}{dT} = \frac{A}{\lambda} e^{-\frac{Ea}{RT}} f(\alpha) \qquad (2)$$

where dx/dT is the non-isothermal reaction rate. Integrating the differential form of non-isothermal equation produces the integral form of non-isothermal rate law (also known as the temperature integral), which is expressed as [45]:

$$g(x) = \frac{A}{\lambda} \int_0^T e^{-\frac{Ea}{RT}} dT \qquad (2.1)$$

Thus, for nonisothermal experiments, each run must be carried out under the same experimental conditions (sample weight, purge gas rate, and sample size), with the heating rate being the only variable. For the experiments, in order to obtain accurate results with high resolution curves low ranges of heating rates should be considered.

4.2.1 Kissinger- Akahira- Sunose equation

The general method of Kissinger [45] uses non-linear mass loss/gain or the release/adsorption of heat in various processes, crystallization, glass transition, and melting to determine the kinetic parameters of the reaction, with respect to reaction temperature. It estimates the activation energy of thermally stimulated processes usually studied by DSC, DTA, and DTG. The Kissinger method is not the best choice when focusing on process kinetics because it yields a single activation energy in agreement with the assumption of single-step kinetics. Isoconversional methods such as Kissinger-Akahira-Sunose (KAS) offer an insightful alternative. KAS is a method of kinetic analysis responsible for calculating dependence of activation energy E(α) on degree of conversion α for dynamic experiments with different constant heating rates β. It is known as one of the most fitting known methods in applying the

approximation of temperature integral to calculate kinetic parameters. KAS uses kinetic parameters to characterize the thermal degradation process of biomass/soot etc. This method uses the Murray and White approximation for temperature integral to propose the following expression:

$$ln\left(\frac{\beta}{T_m^2}\right) = ln\left(\frac{AR}{E_a}\right) - \frac{E_a}{RT_\alpha} \quad (2.2)$$

EXPERIMENTAL

CHAPER 5

Synthesis

Samples were already prepared by combustion synthesis using aluminium nitrate nonahydrate ($Al(NO_3)_3 \times 9H_2O$, p.a. Kemika, Croatia) and cerium nitrate hexahydrate ($Ce(NO_3)_3 \times 6H_2O$, purum, Merck, Germany) as aluminium and cerium precursors and oxidizing agents, glycine (NH_2CH_2COOH, p.a., LACH-NER, Czech Republic) as a fuel, and copper nitrate trihydrate (($Cu(NO_3)_2 \times 3H_2O$,) as a source of copper. Typical synthesis procedure was as follows: 0.04 mol (15.0 g) of $Al(NO_3)_3 \times 9H_2O$, 0.0095 mol (4.12 g) of $Ce(NO_3)_3 \times 6H_2O$, 0.083 mol (6.23 g) of NH_2CH_2COOH and 0.0005 mol of Cu precursor (molar ratio Al:Ce:Cu = 49,5:49,5:1) were dissolved in porcelain bowl in 10 mL of deionized water, heated on hot plate to 60 °C and stirred with magnetic stirrer. Due to water evaporation the viscosity gradually increased and finally mixture become thick enough to stop the magnet, which was then removed, and bowl transferred to sand bath set to a maximal temperature. Beside sample with 1% of Cu, samples with 0, 0.5 and 2 mol % of Cu were prepared maintaining Ce to Al ratio at 1. In this investigation prepared samples were thermally treated at 800 °C for 2 h in order to ensure ceria crystallization and complete removal of organics.

5.1 Carbon black

Carbon black is a substance formed by the incomplete combustion of heavy petroleum products such as coal tar, vegetable matter, and fluid catalytic cracking tar. Carbon black (CB) consists essentially of finely divided, spherical particles of carbon produced by incomplete combustion of carbonaceous fuels, both liquid and gaseous, that are chemically bonded

forming agglomerate chains via weak Van der Waals interactions [46]. CB is mesoporous, with a wide pore size distribution due to the mesoporous structure and the effect of large-chain agglomeration. CB may have applications in areas such as antibody delivery catalyst, supercapacitors , capacitors, UV stabilizers , pigments , concrete additive , paper additive ,rubber additives, plastic additives, coatings and structural reinforcement [46]. CB has a high surface-to-volume ratio due to its small size (usually, below 50 nm) [46]. Usually, the carbon content of CB is greater than 98 percent, but oxygen is always present in trace amounts due to the presence of numerous oxygen-containing functional groups on the nanoparticles' surfaces.

5.1.1 Characterization methods of the synthesized powder

In this study various characterisation methods were employed. These include FTIR, XRD, SEM and DTA-TGA. X-ray diffraction analysis was performed using a Shimadzu XRD 6000 diffractometer with CuKα radiation. FTIR spectrum was obtained using an IR spectrometer and data was obtained in the range of wave numbers from 500 to 4000cm^{-1} and more 64 than scans. Differential thermal (DTA) and thermogravimetric (TGA) analyses were performed on a NETZSCH thermal analyser STA 409. SEM was carried out using a Tescan Vega-3 SEM. The catalytic activity of the prepared samples was tested on the soot oxidation process. Mixtures of thermally treated samples and carbon black in a weight ratio of 4: 1 were prepared for the oxidation of carbon black. In order to achieve good homogeneity, the mixtures were prepared by stirring in a mortar with a small amount of absolute ethanol. After grinding, the mixture was placed in a dryer to remove ethanol. 10 mg of the prepared mixture was placed in an alumina crucible and DTA / TGA analysis was performed in a 100cm^3 / min air stream.

5.1.2 Carbon black/catalyst mixture preparation

Figure 9a shows the powdered sample without copper. 80mg of catalyst thermally treated at 800 °C for 2 h and 20mg of activated carbon is mixed with a mortar and pestle as shown in Figure 9b. below, in a presence of a few ml of ethanol and then homogenized until dry. This is repeated two times more and then the dry powder is stored As represented in Figure 9c samples with 0, 0.5, 1 and 2% Cu already prepared by combustion synthesis are used in this study. It is observed that at different concentrations of copper the volume of the samples appear different. When there is more copper the volume of sample appears smaller. The mass remains the same

but the density varies. Therefore more copper results in higher density and smaller volume. Non isothermal TGA of dried samples are observed. The heating rate of the samples were 2.5 5, 7.5, and 10 °C/min as represented in Table 2 below. This also includes recorded masses of the samples containing carbon with catalyst and carbon without catalyst are shown before thermal treatment. At the end of the experiment, 15 TGA scans (conditions optimization,2 samples + carbon without catalyst, 4 heating rates) were obtained.

Table 2. Mass measurements from lab experiments

Flowrate 100ml/min			
Mv(Crucible)= 0.1453g=145.3mg			
Mv(Sample)=9.9mg			
Sample	Heating rate° /min	Empty crucible mass/mg	Sample mass /mg
CB	1.0	145.5	10.0
CB	2.0	145.6	9.8
CB	2.5	145.7	9.9
CB	5.0	145.3	9.9
CB	7.5	146.7	9.9
CB+Catalyst(with Cu)	2.5	145.7	10.1
CB+Catalyst(with Cu)	5.0	145.8	9.8
CB+Catalyst(with Cu)	7.5	145.6	9.9
CB+Catalyst(with Cu)	10.0	145.9	10.0
CB+ Catalyst (without Cu)	2.5	145.8	9.9
CB+ Catalyst(without Cu)	5.0	145.7	9.8
CB+ Catalyst(without Cu)	7.5	145.7	9.8
CB+ Catalyst(without Cu)	10.0	145.8	10.0

(a) (b) (c)

Figure 9. a)Cerium oxide catalyst b)Carbon black mixing c) Prepared mixtures of CB and catalyst

5.2 TGA-DTA

Thermal analysis is the analysis of a change in a property of a sample, which is related to an imposed change in the temperature [47]. The sample is usually solid, and heating causes changes such as melting, phase transition, sublimation, and decomposition. Thermogravimetric analysis is the study of how a sample's mass changes when heated (TG). This mass variation can be a loss of mass (vapour emission) or a gain of mass (gas fixation). Under a controlled atmosphere, TG measures mass changes in a material as a function of temperature (or time). Its primary applications include determining the thermal stability and composition of a material. TG is most useful in the processes of dehydration, decomposition, desorption, and oxidation. Differential thermal analysis (DTA) is a commonly used thermal analysis method. During a programmed temperature change, the temperature of a sample is compared to that of an inert reference material in DTA. The temperature should remain constant until a thermal event, such as melting, decomposition, or a change in the crystal structure, occurs. When an endothermic event occurs within the sample, the temperature lags behind that of the reference, and a minimum is observed on the curve. In contrast, if an exothermal event occurs, the temperature of the sample will exceed that of the reference, resulting in a maximum on the curve. The enthalpy is proportional to the area under the endotherm. Many problems benefit from using simultaneously DTA and TGA, because DTA events can then be classified as involving or not involving mass change. In DTA the ideal reference material is a substance

with the same thermal capacity as the sample, but without thermal events above the temperature range of interest. Therefore, alumina (Al_2O_3), silicon carbide (SiC) or magnesium oxide (MgO) powder are usually used as the reference material for the analysis of inorganic compounds. Aforementioned thermogravimetry's main objective is to measure the mass of sample as a function of temperature, determine sample purity, decomposition behaviour, chemical kinetics (resulting in changes of mass such as absorption, adsorption, desorption) [48]. In this study, Thermogravimetric Analysis (TGA) was determined from room temperature to 800 °C, with various heating rates and nitrogen atmosphere with an air flow speed of 100 mL min^{-1}. Figures 10. and 11. show a schematic of such analysers used to evaluate thermal stability of a given sample. A brief summary of the procedure is shown in Table 3 below.

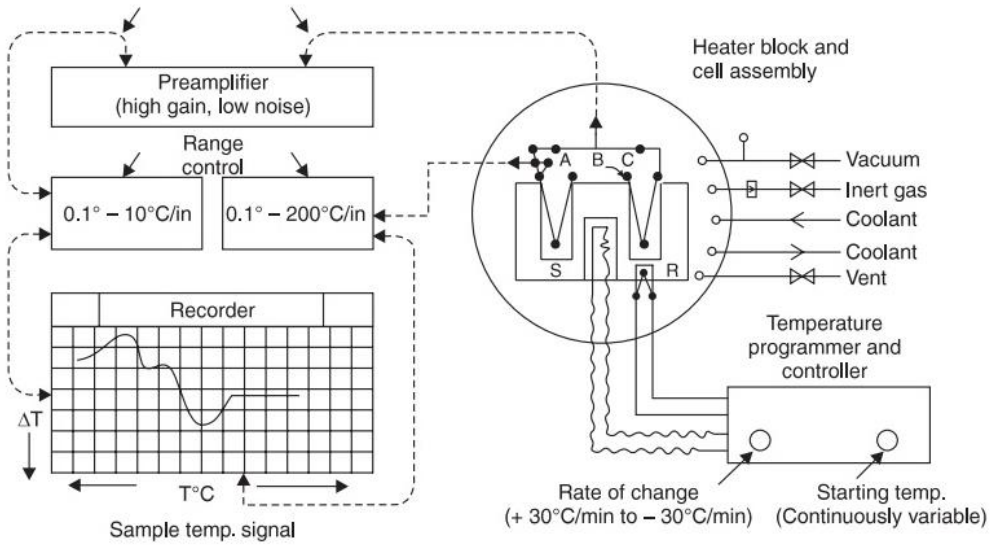

Figure 10. Schematic diagram of a Differential Thermal Analyzer (E.I Du Pont De Nemours, Inc, USA) [49]

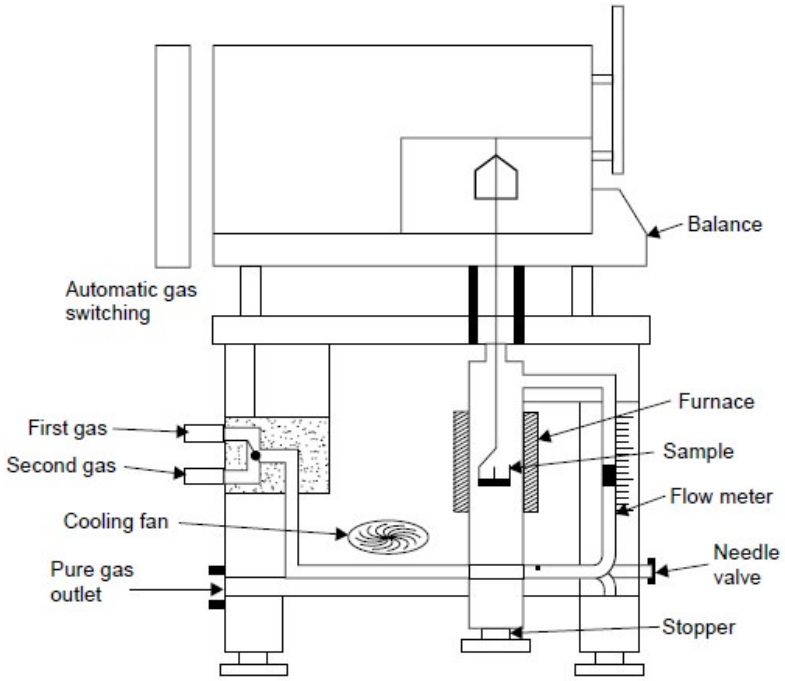

Figure 11. Thermobalance for Thermogravimetric Analysis in a Controlled Atmosphere up to 1000 °C [49]

Table 3. Summary of DTA-TGA analysis [49]

APPLICATION	DTA	TGA
THEORY	Measure the mass of sample	Measure temperature difference between reference and sample
MASS CHANGE	Yes	No
QUALITATIVE ANALYSIS OF HEAT CHANGE	No	Yes
QUANTITATIVE ANALYSIS OF HEAT CHANGE	No	No

5.2.1 FTIR

The range of wavelengths in the infrared region absorbed by a substance is measured using FTIR analysis. This is achieved by exposing samples of a material to infrared radiation (IR). The ability of a sample to absorb the energy of infrared light at various wavelengths is measured in order to determine the material's molecular composition and structure. Unknown materials are found by comparing the spectrum to a database of reference spectra, as long as a standard curve of known concentrations of the component of interest can be established. FTIR Analysis can be used to identify unknown materials, polymer additives, surface contamination on a material, and other things. The results of the tests can be used to determine the molecular composition of a sample. (FTIR) analysis were made using a Bruker Vertex 70 IR spectra in ATR mode.

5.2.2 XRD

X-ray diffraction (XRD) is a powerful non-destructive technique for characterizing crystalline materials [50]. It can analyse a wide range of materials including fluids, metals, minerals, polymers, catalysts, pharmaceuticals, thin-film coatings, ceramics, solar cells, and semiconductors. It provides information on structures, phases, preferred crystal orientations (texture), and other structural parameters, such as average grain size, crystallinity, strain, and crystal defects [50]. Constructive interference of a monochromatic beam of X-rays scattered at specific angles from each set of lattice planes in a sample produces X-ray diffraction peaks. The distribution of atoms within the lattice determines the peak intensities. As a result, the X-ray diffraction pattern is the fingerprint of a material's periodic atomic arrangements. Afterwards, the diffracted X-rays are detected, processed, and counted. Due to the random orientation of the powdered material, all possible diffraction directions of the lattice should be attained by scanning the sample through a range of 2θ angles. Because each compound has a unique set of d-spacings, converting the diffraction peaks to d-spacings allows identification of the compound. This is typically accomplished by comparing d-spacings to standard reference patterns. Copper is the most common target material for single-crystal diffraction, with CuK_α radiation λ=1.5418 Å [50]. These X-rays are collimated before being directed at the sample. The intensity of the reflected X-rays is measured as the sample and detector are rotated. When the incident X-rays impinging on the sample satisfy Bragg's law, constructive interference occurs and a peak in intensity appears. This X-ray signal is recorded and processed

by a detector, which converts it to a count rate, which is then recorded and output to a device such as computer monitor.

5.2.3 SEM

A SEM image is formed in an electron gun through a beam of electrons (~100 nA) produced by either thermionic or field emission mechanisms [51]. Primary electrons bombard surface of the sample under investigation to produce secondary electrons through the inelastic collision of primary electrons and valence electrons orbiting the nucleus of the samples' atoms [51]. A set of electromagnetic lenses guides the beam of electrons to the raster sample surface, while a scanning coil controls the spot size of the electron beam. A secondary electron detector is used to collect them and use them in image formation. Backscattered electrons are produced by elastic collisions between primary electrons and the nucleus of the sample atoms and can be collected using a backscattered electron detector to produce an image with differentiable contrast in regions with high atomic number element concentrations compared to those with low atomic number element concentrations. X-ray signals are also generated and used for chemical identification of materials on atom surfaces (EDS). Therefore, by using SEM coupled with EDS it is possible to observe and characterize the sample in terms of its (1) surface morphology, (2) structural organization, and (3) chemical composition [52]. The vacuum of the SEM needs to be below 10^{-4} Torr (0.013Pa) to operate, although most microscopes operate at 10^{-6} Torr (0.00013Pa) or greater vacuum [51]. SEM analysis is non-destructive which means that x-rays produced by electron interactions do not lead to loss of volume of the samples thus the same samples can be analysed repeatedly. Figure 13 shows the SEM equipment used during analysis of one of the samples containing copper doped ceria. During imaging, electrons are constantly bombarding the sample, and a negative charge can accumulate in areas of the sample under the beam. This negative charge, when sufficiently large, can deflect the incident and emitted electrons, thus ruining the image so exposure of nonconductive samples to an electron shower results in electrical charging of the sample culminating a useless image with glaring spots). In general, the samples examined in an SEM must be electrically conductive to minimize charge build-up on the sample caused by the electron beam [52]. To avoid this issue deposition of 100 A˚ gold or carbon coating is done as shown in Figure 14 below. Furthermore, to ensure the electrical contact between this conductive layer and the metallic holder of the sample, a conductive silver or carbon ink or tape is used, ensuring good grounding of the sample as shown on Figure 12.

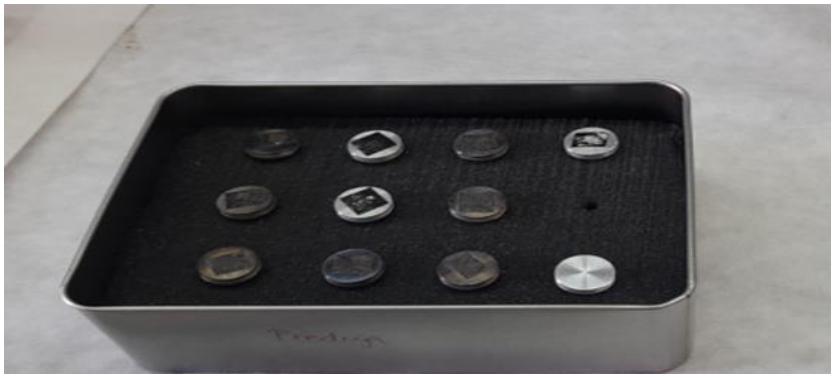

Figure 12. SEM sample holder with conductive tape

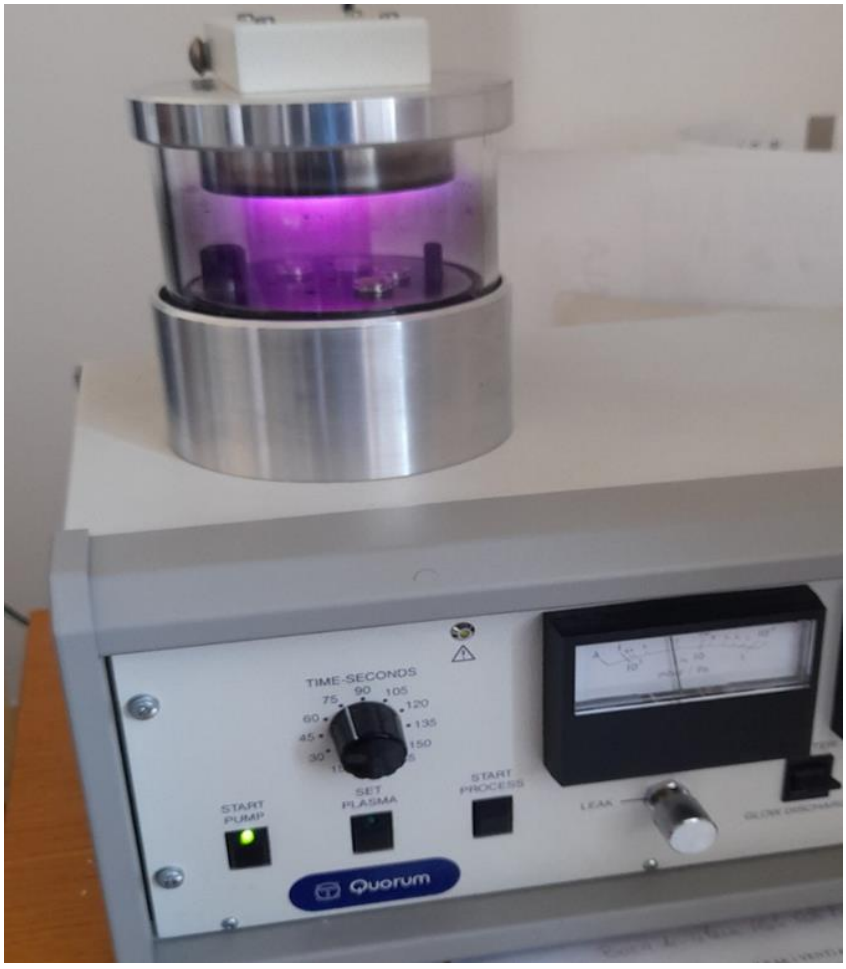

Figure 13. Sputter

CHAPTER 6

6.1 RESULTS AND DISCUSION

6.1.1 XRD Results

.

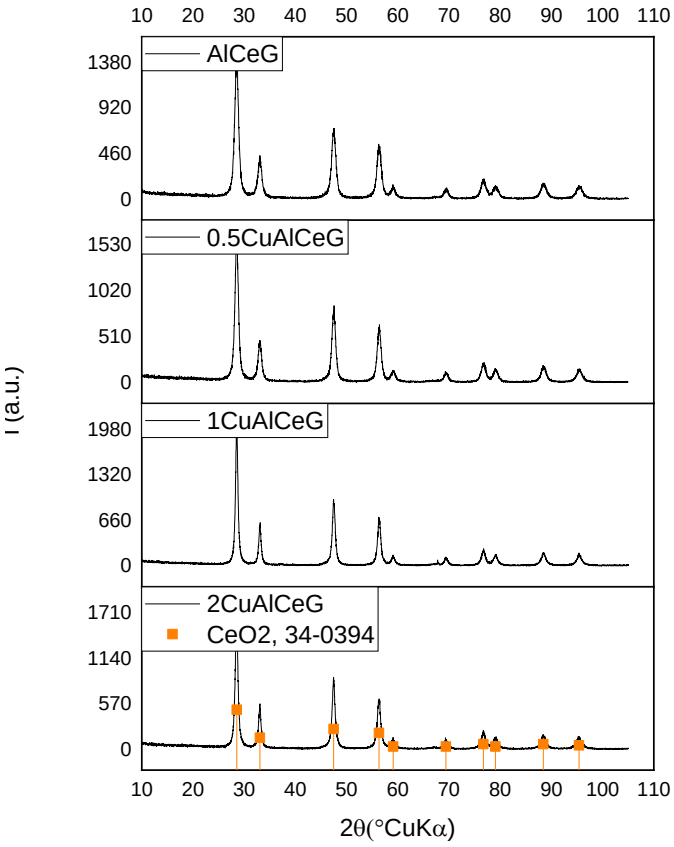

Figure 14. XRD patterns

Figure 14 depicts the XRD patterns of the catalyst after a 2-hour heat treatment at 800 ° C. All of the samples showed the characteristic peaks of a fluorite-type cubic phase of CeO_2 (space group Fm-3m). Characteristic peaks can be observed at 2θ values of 28 °, 34 °, 55 °, and 56 ° which correspond to CeO_2 (111), (200), (311) and (222) lattice planes respectively. No separate phase of Cu containing compound in doped samples has been noted. Amount of copper in samples is relatively small so it could be invisible to XRD. On the other hand, it is possible that it entered crystal lattice of ceria. Also, no clear peaks of γ-Al_2O_3 could be observed. although, considering a large amount of Al in sample it is clear that it is present in some form. That could be due to great differences in cerium and aluminium scattering factors but also there

is a possibility that alumina is in amorphous state and thus invisible for XRD. A narrower diffraction maximum indicating larger crystallites have been noted for doped samples.

6.2 X-ray diffraction analysis results

Crystalline size can be determined by Sherrer method. Relationship of the diffraction maxima width on crystallite size is defined by Scherrer equation:

$$L = \frac{K\lambda}{\beta cos\theta} \qquad (6)$$

where L is the size of crystallites in nanometres, Θ Bragg angle of diffraction maxima in °Θ, λ is the wavelength of the incidence X-rays in nm, K is a constant and its values are usually between 0.85 and 0.99, β is the width of the peak on the half of its height after the correction due to the instrumental broadening expressed in radians. If the width of the diffraction maximum is determined by refinement to the Lorentz function, β is defined by the equation:

$$\beta = \beta_o - \beta_i \qquad (6.1)$$

where β o is the observed width at half height and β i the expansion due to the characteristics of the instrument

Table 4. Scherrer method values

SAMPLE	K	β (radians)	θ (radians)	λ (nm)	L(nm)
AlCeG	0.94	0.0131	0.415	0.15405	11.1
0.5CuAlCeG	0.94	0.0114	0.415	0.15405	12.7
1CuAlCeG	0.94	0.0082	0.415	0.15405	17.7
2CuAlCeG	0.94	0.0087	0.415	0.15405	16.6

Table 4 lists the crystallite sizes for samples with 0,0.5, 1 and 2% Cu determined by the Scherrer method. Sample with 2CuAlCeG exhibited the smallest crystallite size whilst AlCeG showed a greater crystallite size. Smaller crystallite size can be attributed to the increased dopant concentration found in the sample due to interference with diffusion and lattice distortion. This results in grain growth inhibition.

6.3 FTIR results

Table 5. Characteristic IR bands in investigated samples

BAND	ELEMENT
2358 and 2340 cm-1	CO_2
1630 and 3400cm-1	H-O-H bending (presence of H_2O)
below 700 cm-1	Ce – O bending
1380 cm-1	Ce-O-Ce vibrations characteristic of the fluorite cubic structure of CeO_2
850, 1060, 1320 and 1415, 1540 cm-1	Bands characteristic of carbonates (adsorption on CeO_2 - small crystallites, large specific surface area)
620 cm-1	Al-O bonds in amorphous materials characteristic of materials obtained by combustion synthesis
518 cm-1	γ-Al_2O_3, i.e., Al (IV) -O vibrations

[53][53]

Table 5 shows results of the spectra analysis from previous studies that can be compared to that of Figure 15, which shows FTIR spectra of investigated samples. The infrared spectrum (FTIR) of the synthesized CeO_2 nanoparticles was in the 400-4000 cm^{-1} wavenumber range, identifying the chemical bonds and functional groups in the compound. The bands at 3400 and 1620 cm^{-1} are stretching vibrations of O-H due to a presence of adsorbed water on surface nanoparticles and can be found in all the graphs despite being weak. Furthermore, the observed band in all graphs at around 400 cm^{-1} was related to the stretching vibration of Ce-O-O. Despite being weak the CO_2 asymmetric stretching vibration, $C0_3^{2-}$ bending vibration, and C-O stretching vibration have been assigned to the bands located around 741, 750, and 1036 cm^{-1}, respectively. Table 6 lists the possible bands obtained by FTIR analysis as stated by Mokkel et

al. [53]. These could be used as possible references of the synthesized samples. They also observed Ce-O elongation, CO_2 adsorbed on the surface (at 2410 cm^{-1} in their work) [53], and H-O-H elongation. As observed, all samples indicate presence of Ce-0 and Al-O bonds with slightly different intensities.

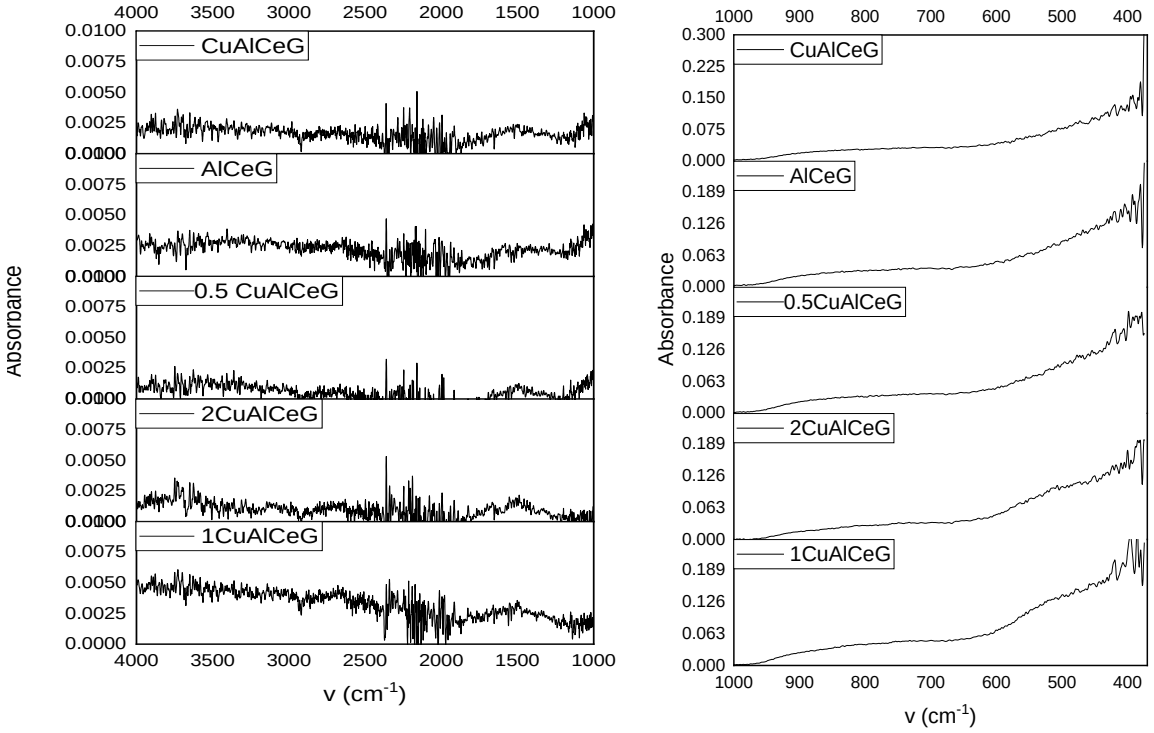

(a) (b)

Figure 15. FTIR sample measurements in the ranges (a) 1000-4000cm^{-1} (b) 400-1000cm^{-1}

6.4 SEM results

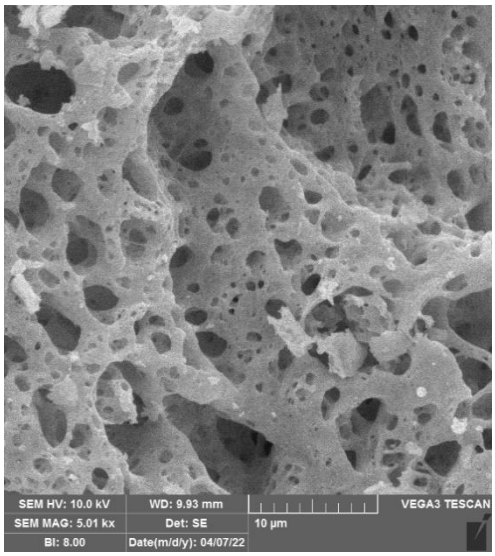

(a)

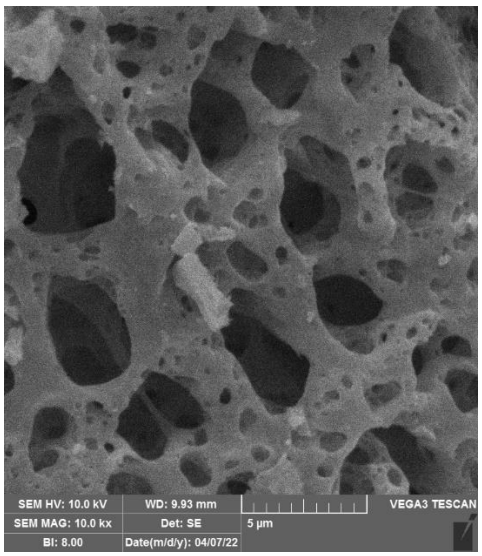

(b)

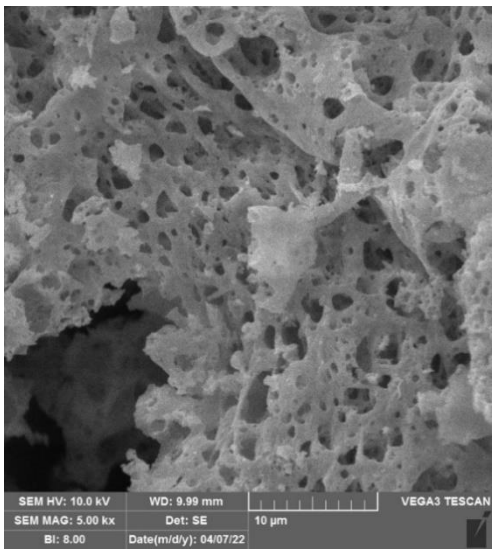

(c)

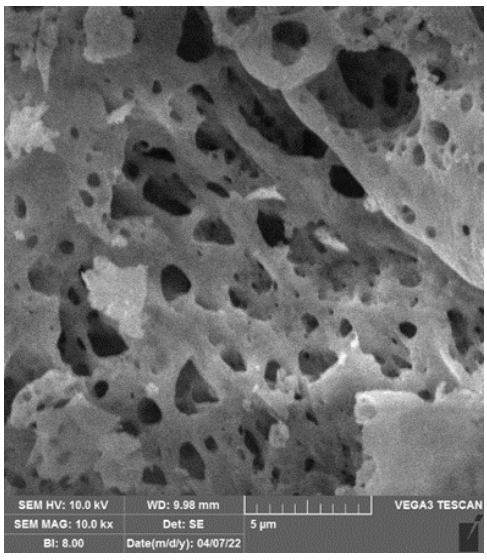

(d)

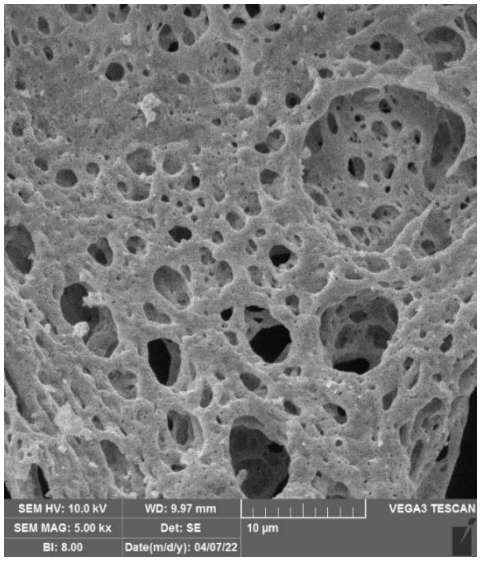

(e)

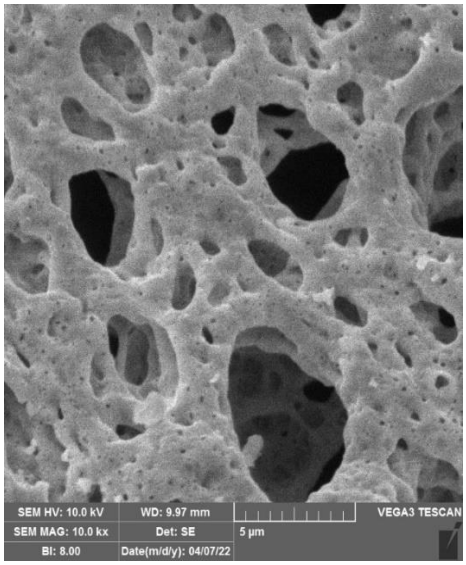

(f)

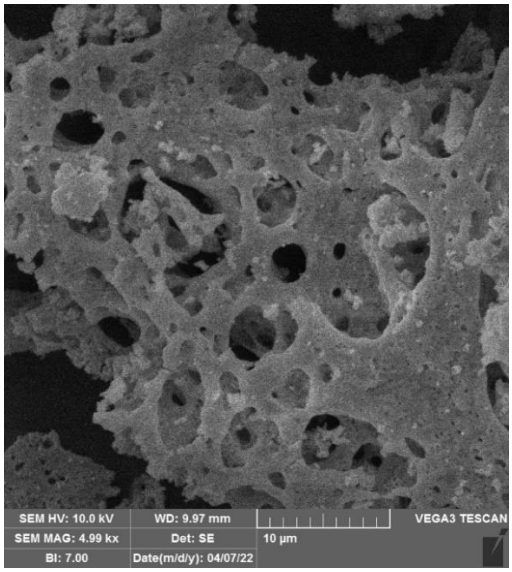

(g)

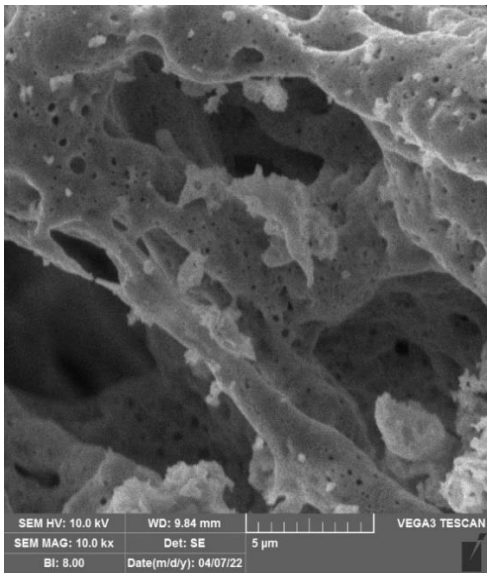

(h)

Figure 16. Micrographs of (a)AlCeG at magnification of 5000 x (b) AlCeG at 10000 x (c)0.5CuAlCeG at 5000 x (d) 0.5CuAlCeG at 10000 x (e) 1CuAlCeG at 5000 x (f) 1CuAlCeG at 10000 x (g) 2CuAlCeG at 5000 x (h) 2CuAlCeG at 10000x

SEM analysis was used to gain insight into morphology of samples. In Figures 16 (a-h) the SEM micrographs of investigated samples are shown. Only sporadically some sphere- shaped

particles are visible. The majority of each sample is composed of agglomerates with sponge-like morphology.

CHAPTER 7

7.1 TGA-DTG Analysis

DTG curves

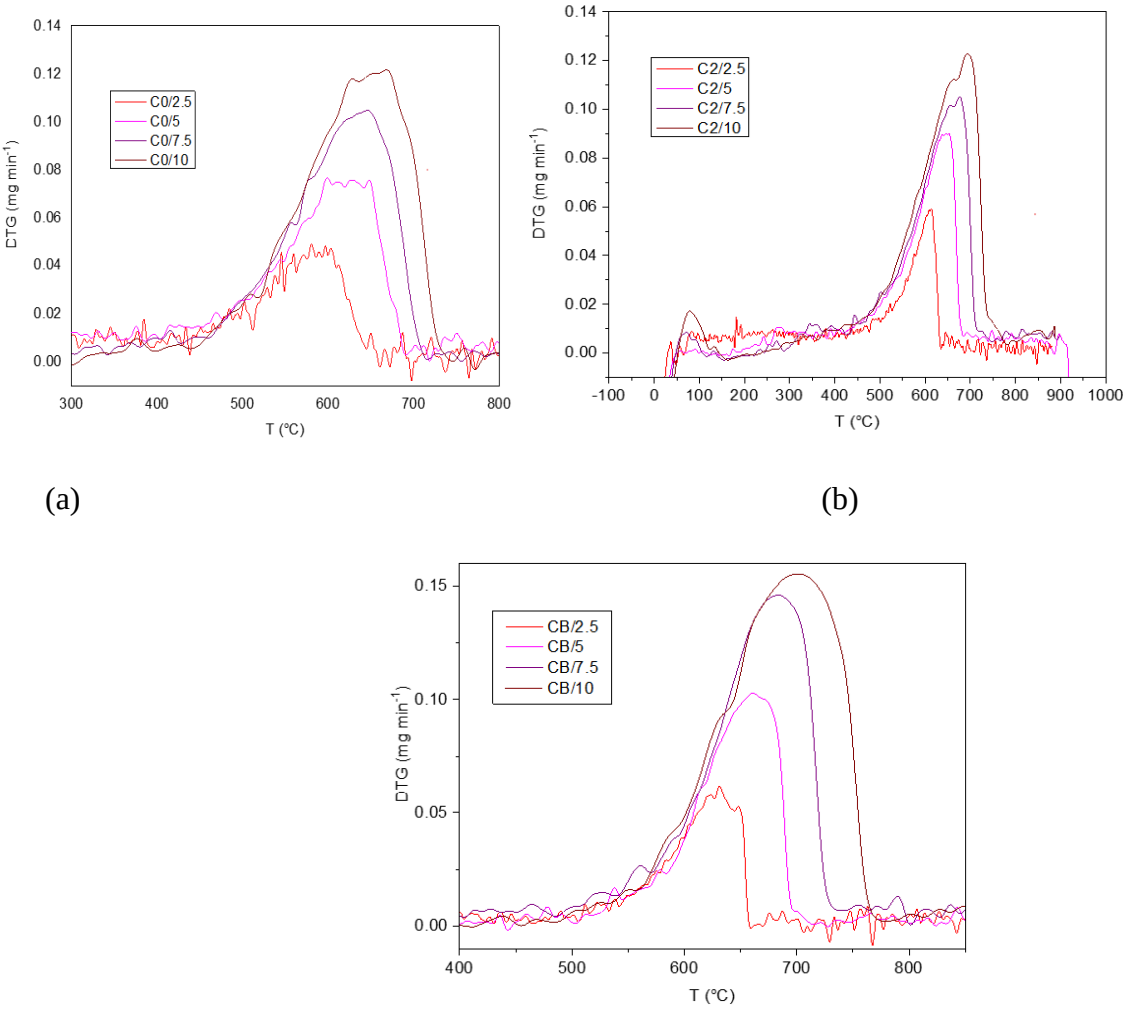

(a) (b)

(c)

Figure 17. DTG curves of (a) CuAlCeG with carbon (b) CuAlCeG without carbon (c) Carbon black (no catalyst)

DTG curves can be used for precise determination of the onset and offset of temperature interval for carbon oxidation and carbonate decomposition. The transfer of oxygen molecules to the soot surface is usually the limiting step of the overall reaction rate at high reaction temperatures. However, at lower temperatures, the reaction is most likely under control of the reaction at the interface. Graphs show there is an improved oxidation activity when catalyst is added (Figures X a and X b) in comparison to the oxidation of pure carbon black (Figure X c).

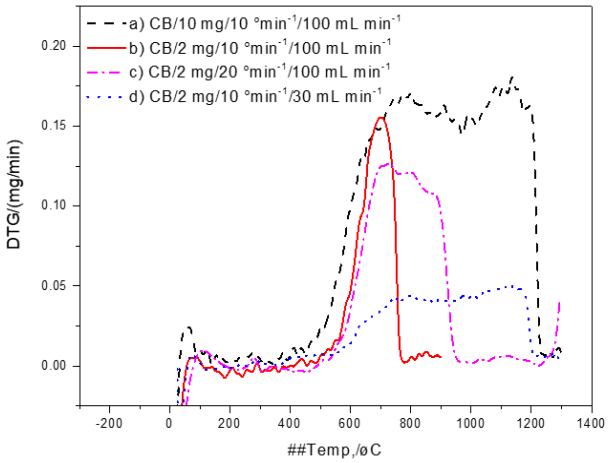

Figure 18. DTG curves obtained with different soot oxidation conditions

Figure 18 above shows four DTG curves obtained under different soot oxidation conditions: a) 10 mg of pure carbon black with 10 °C min^{-1}heating rate and 100 mL min^{-1} air flow rate. The use of 10mg produces a curve with double peaks this is due to diffusional limitations. Taking into consideration temperature span, heating rate, air flow rate due to mass transfer and oxygen availability, oxygen content in the air and sample mass, it appears that that the amount of oxygen flowing through the furnace is far greater than the amount of carbon required by stoichiometry. Therefore, the behaviour exhibited could be attributed to oxygen transfer limitations. Diffusional limitations also produce double peaks for curves obtained with far lesser mass of 2 mg but having smaller ait flow rate of 30 mL min^{-1}, as well as greater heating rate. Smaller mass, greater air flow and limitation of heating rate to 10 °C min^{-1} yield with single peak, which is an indication that the diffusion limitations were avoided. Two mechanisms control the process when a double peaked curve is obtained,

reaction on the interface and diffusion. To avoid limiting factors that made diffusion controlling process, air flow rate has to be increased, heating rate decreased, and smaller mass used.

TGA curves

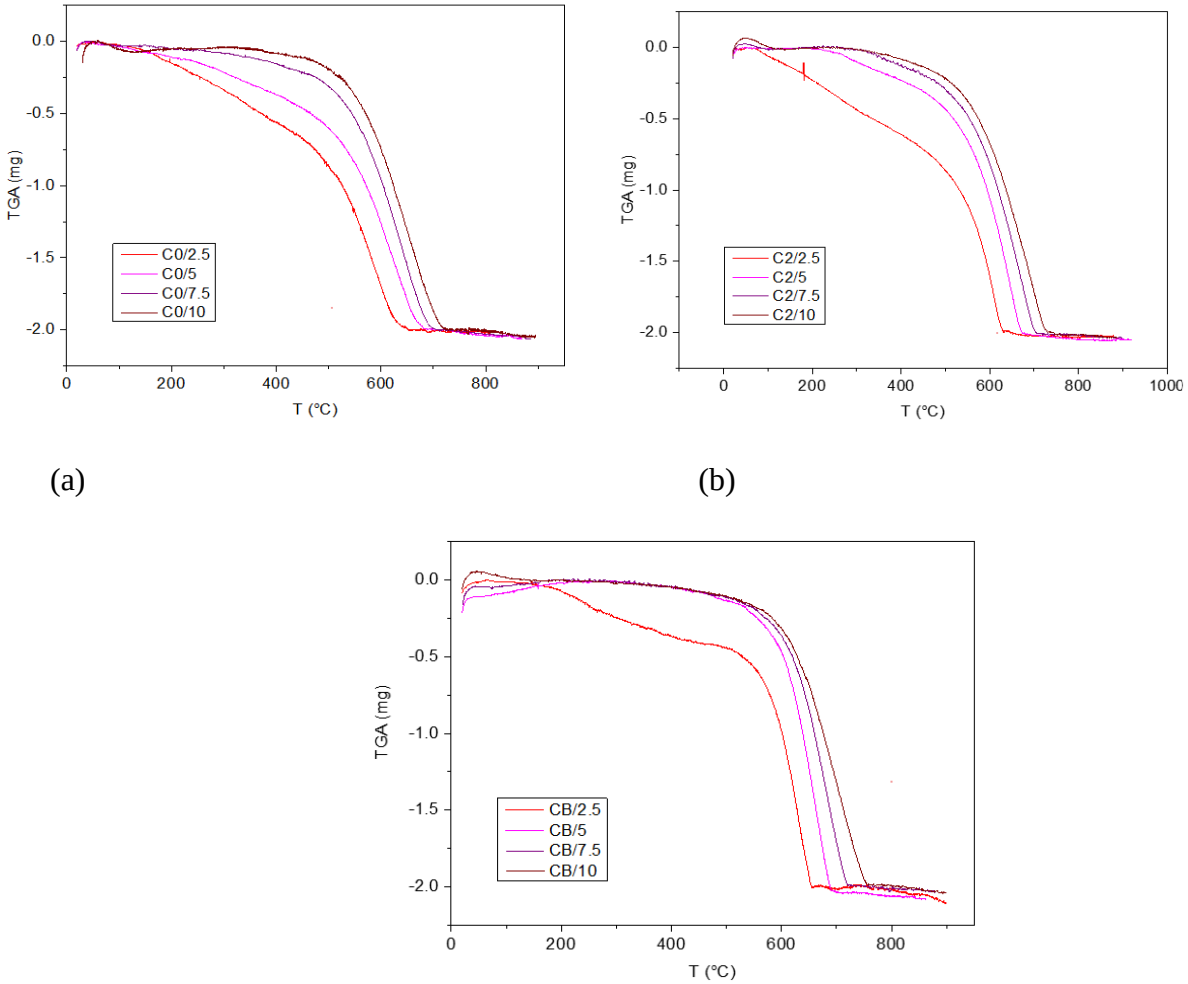

Figure 19. TGA curves of (a) CuAlCeG with carbon (b) CuAlCeG without carbon (c) Carbon black (no catalyst)

The TGA curves shown in Figure 19 demonstrate the thermal behaviour of the catalyst-soot. Heat treatment is done at various temperatures. When compared to samples without catalyst, all samples with catalysts showed increased rate of carbon soot oxidation. CeCu catalysts exceeded CeAl samples in terms of catalytic performance. Despite having slightly lower

catalytic activity than other Ce-based nanocomposites, copper is a less expensive element when compared to other dopants such as zirconium, lanthanum, and praseodymium.

7.2 Kinetic analysis based on TGA curves

Kinetics Analysis Based on Nonisothermal Experiments

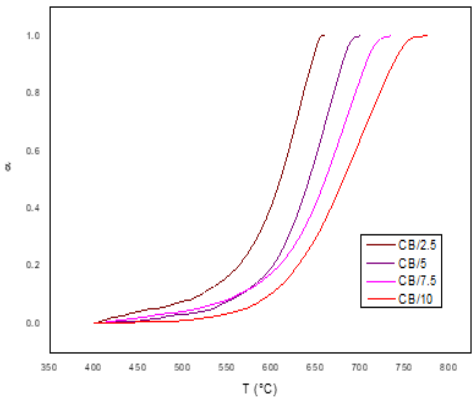

(a)

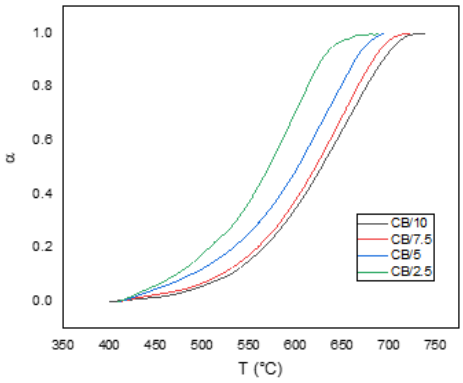

(b)

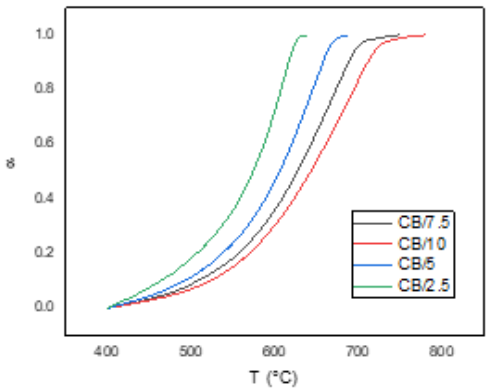

(c)

Figure. 20 Conversion vs. temperature curves for (a) pure CB oxidation obtained at different heating rates; (b) CB oxidation with catalyst (CuAlCeG) obtained at different heating rates (c) CB oxidation with catalyst (2CuAlCeG) obtained at different heating rates

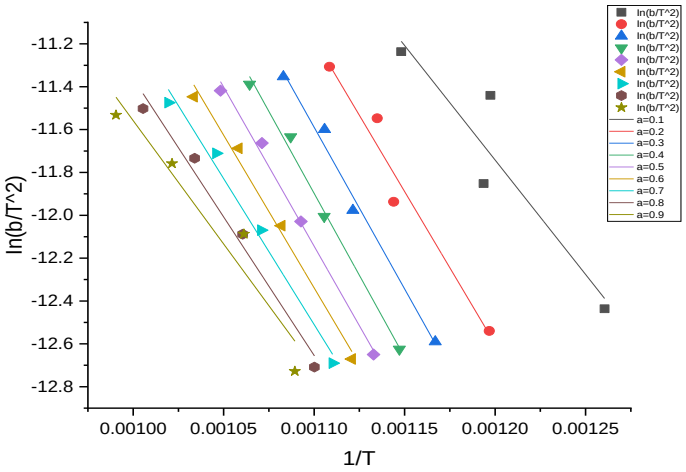

(a)

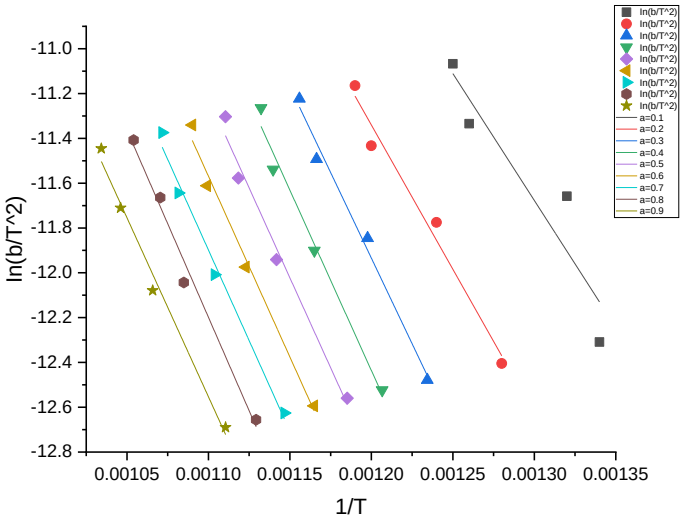

(b)

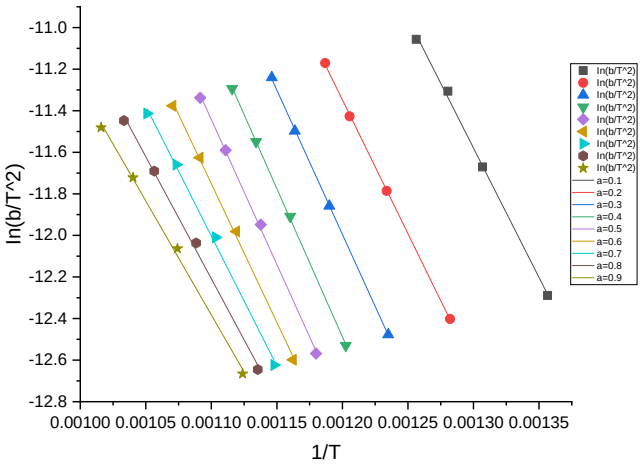

(c)

Figure 20. KAS plots for (a) non-catalytic oxidation of pure CB, (b) catalytic oxidation of CB with catalyst (CuAlCeG) (c) catalytic oxidation of CB with catalyst (2CuAlCeG)

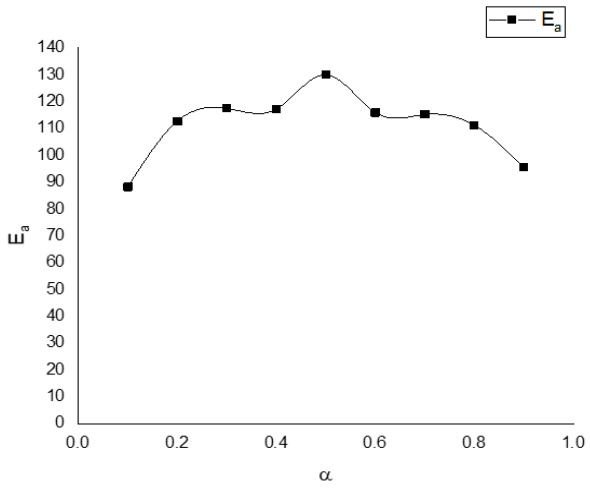

(a)

ALPHA	ACTIVATION ENERGY (kJ/mol)
0.1	88.27
0.2	112.8
0.3	117.57
0.4	117.3
0.5	130.1
0.6	116.0
0.7	115.23
0.8	111.23
0.9	95.67

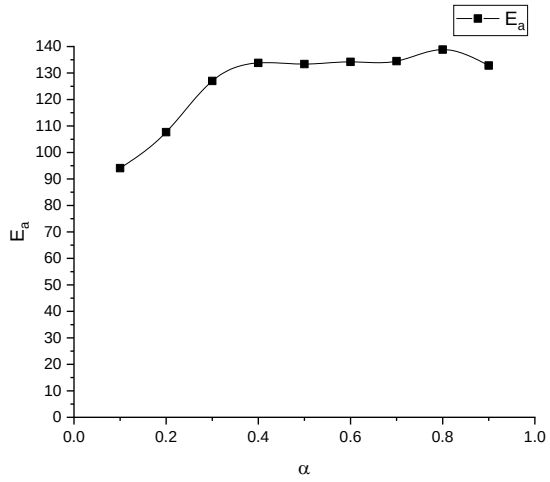

ALPHA	ACTIVATION ENERGY (kJ/mol)
0.1	94.1
0.2	107.66
0.3	127.02
0.4	133.82
0.5	133.39
0.6	134.20
0.7	134.51
0.8	138.84
0.9	132.83

(b)

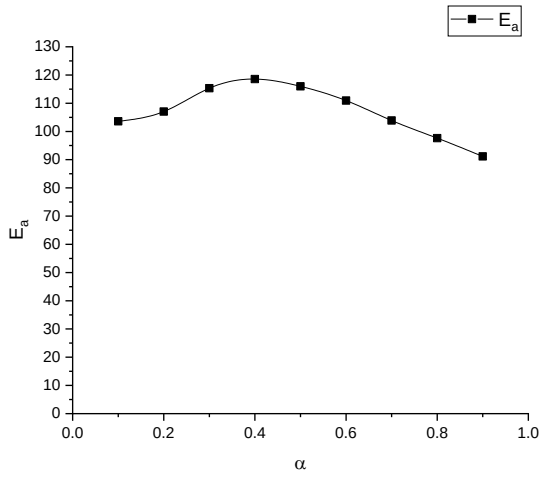

ALPHA	ACTIVATION ENERGY (kJ/mol)
0.1	103.58
0.2	107.06
0.3	115.32
0.4	118.56
0.5	115.97
0.6	110.93
0.7	103.9
0.8	97.63
0.9	91.15

(c)

Figure. 21 Activation energy vs. conversion plots for (a) pure CB (b) CB with catalyst (CuAlCeG) (c) CB with catalyst (2CuAlCeG)

The conversion–temperature curves for CB with and without catalyst are recorded at various constant heating rates are shown in Figure 20 a-c. When the isoconversional kinetic analysis method was applied, the apparent activation energy (E_a) was determined from the slope of ln (β/ T_x^2) versus 1/T at a constant α value (α is the conversion). The corresponding results are shown in Figure 21 a-c.

The temperature conversion curves exhibited a clear dependence on heating rate, with conversion curves shifting to higher temperatures at higher heating rates. The activation energies and pre-exponential factors were calculated at various degrees of conversion, and it was discovered that the activation energy varied with the extent of conversion, ranging from 88.27 kJ/mol to 138.85 kJ/mol, with a mean value of 114 kJ/mol. The sample containing CB and catalyst mixture (2CuAlCeG) shows the most constant decline in E_a results from 103.58Kj/mol to 91.15kJ/mol. The highest E_a values are observed in the sample containing pure CB without catalyst, it reaches 138.84kJ/mol at 0.8 conversion. Su et al. mentioned that the apparent dependence of activation energy on conversion indicated that the assumption of a single-step reaction is not accurate enough in the case soot oxidation(Su et al., 2018). However, the kinetic parameters for soot oxidation cannot simply be compared from one study to another due to the differences in the nature of the soot and the experimental conditions of the reactors (i.e., the mass and heat transfer limitations)[54].

CHAPTER 8

8.1 CONCLUSION

The catalytic oxidative properties of CeO_2, and CeO_2 with 2 % of copper in reaction with soot at different heating rates of 2.5, 5, 7.5, and 10°C/min were investigated. Materials containing nanocrystalline ceria have shown to be suitable catalysts. This is attributed to the improvement of both the oxygen vacancy concentration and the oxygen storage capacity, as well as the redox activities. The oxidation of soot is an example of a successful application of the CeO_2-Cu system. Ceria's redox property makes it suitable for use as a catalyst or support in chemical reactions. It is known that modifying ceria with various cations affects oxygen mobility, which is important in catalytic soot combustion and improves sintering stability and oxidation activity of the resulting catalysts. Changes in redox properties and the formation of oxygen vacancies result from this modification, both of which improve the oxygen exchange capacity between the gas phase and the catalyst as well as its oxygen storage capacity. The oxygen atoms/vacancies attached to reducible elements are mobile and contribute to the mixed oxides' oxygen storage/release capacity, and thus to their oxidation activity. Doping CeO_2 with dopants with valences lower than 4+ is intended to create oxygen vacancies in the CeO_2 structure, as opposed to the more traditional doping of CeO_2 with ZrO_2, which is intended to increase thermal stability. The properties of oxygen vacancies, such as local atomic structure, chemical environment, and binding energies, can be controlled in principle by the dopant used. Incorporation of Cu influenced the synthesis process, the Cu doped ceria catalysts demonstrated enhanced activity in soot oxidation with complete combustion, as expected, when compared to pure CeO_2 materials. 2% Cu exhibited the highest catalytic activity, followed in the series by the pure CeO_2. As this study adds to the evidence of a synergetic effect between the active phase of transition metal oxide and the ceria support, as the activity of the doped catalysts exceeds that of pure CeO_2. Comparing the overall soot oxidation results and following kinetic analysis it appears that the use of this doped catalyst yielded greater oxidation rates but in comparison to other catalysts no significant difference has been observed.

REFERENCES

[1] J. Xi and B. J. Zhong, "Soot in diesel combustion systems," *Chemical Engineering and Technology*, vol. 29, no. 6. pp. 665–673, Jun. 2006. doi: 10.1002/ceat.200600016.

[2] "Euro 1 to Euro 6 guide." (2019) Available at: https://www.rac.co.uk/drive/advice/emissions/euro-emissions-standards/ (accessed Jun. 01, 2022).

[3] G. Kastrinaki, S. Lorentzou, and A. G. Konstandopoulos, "Soot Oxidation Kinetics of Different Ceria Nanoparticle Catalysts," *Emission Control Science and Technology*, vol. 1, no. 3, pp. 247–253, Jul. 2015, doi: 10.1007/s40825-015-0021-z.

[4] H. Huang, J. Liu, P. Sun, S. Ye, and B. Liu, "Effects of Mn-doped ceria oxygen-storage material on oxidation activity of diesel soot," *RSC Advances*, vol. 7, no. 12, pp. 7406–7412, 2017, doi: 10.1039/c6ra27007g.

[5] "Diesel engine." (2020) Available at: https://en.wikipedia.org/wiki/Diesel_engine (accessed Jun. 01, 2022).

[6] N. Hemmerlein, V. Korte, H. Rchter, G. Schroeder, "Performance, Exhaust Emissions and Durability of Modern Diesel Engines Running on Rapeseed Oil," *SAE International*, vol. 1, Feb. 1999.

[7] Reif K, editor. Diesel engine management. Springer Vieweg; 2014.https://doi.org/10.1007/978-3-658-03981-3_19.

[8] I. A. Reşitoglu, K. Altinişik, and A. Keskin, "The pollutant emissions from diesel-engine vehicles and exhaust aftertreatment systems," *Clean Technologies and Environmental Policy*, vol. 17, no. 1. Springer Verlag, pp. 15–27, Jan. 04, 2015. doi: 10.1007/s10098-014-0793-9.

[9] World Health Organization. Health Aspects of Air Pollution with Particulate Matter, Ozone and Nitrogen Dioxide Report on a WHO Working Group Ozone-adverse effects Nitrogen Dioxide-adverse effects Air pollutants, Environmental-adverse effects Metal-analysis Air-standards Guidelines, 2003.

[10] O. Meredith, "Passive Catalytic Soot Oxidation," Doctoral dissertation, Cardiff University, 2017.

[11] D. Dwivedi, A. K. Agarwal, and M. Sharma, "Particulate emission characterization of a biodiesel vs diesel-fuelled compression ignition transport engine: A comparative study,"

Atmospheric Environment, vol. 40, no. 29, pp. 5586–5595, Sep. 2006, doi: 10.1016/j.atmosenv.2006.05.005.

[12] D. B. Kittelson, "Engines and Nanoparticles: review," Journal of aerosol Science, vol. 29, no.5-6, pp. 575-588, June 1998.

[13] B. A. A. L. van Setten, M. Makkee, and J. A. Moulijn, "Science and technology of catalytic diesel particulate filters," *Catalysis Reviews - Science and Engineering*, vol. 43, no. 4. pp. 489–564, Nov. 2001. doi: 10.1081/CR-120001810.

[14] J. de Ruyck, *Characteristics of Particle Mass Concentrations from Small Scale Biomass Combustion: A Review*. VII International conference on Energy and Environment for 21 Century, Central University, "Marta Abreu" Kas Villas, Cuba, 2012. [Online]. Available: https://www.researchgate.net/publication/328190906.

[15] G. A. Stratakis, "Experimental Investigation of Catalytic Soot Oxidation and Pressure Drop Characteristics in Wall-Flow Diesel Particulate Filters." Doctoral dissertation, University of Thessaly, 2004

[16] Atif Rashid, "Fix my car," *https://www.fixmycar.pk/toyota-diesel-particulate-filter-dpf-delete/?utm_source=rss&utm_medium=rss&utm_campaign=toyota-diesel-particulate-filter-dpf-delete*, Feb. 15, 2022.

[17] Grzegorz Gurdek, "Otomatik." https://otomatic.eu/construction-and-principle-of-operation-dpf/ (accessed Jun. 22, 2022).

[18] Y. Deng, X. Wang, G. Chen, H. Wu, Z. Han, and R. Li, "Experimental Study on a Diesel Particulate Filter with Reciprocating Flow," *ACS Omega*, vol. 4, no. 17, pp. 17098–17108, Oct. 2019, doi: 10.1021/acsomega.9b01164.

[19] W. R. Wade, J. E. White, and J. Florek, "Diesel Participate Trap Regeneration Techniques," Paper No. 810118. Society of Automative Engineers, Detroit, Michigan,1981.

[20] A. Raj, S. Y. Yang, D. Cha, R. Tayouo, and S. H. Chung, "Structural effects on the oxidation of soot particles by O2: Experimental and theoretical study," *Combustion and Flame*, vol. 160, no. 9, pp. 1812–1826, Sep. 2013, doi: 10.1016/j.combustflame.2013.03.010.

[21] N. K. Labhsetwar *et al.*, "Current Science Association Application of catalytic materials for diesel exhaust emission control," 2004. [Online]. Available: https://about.jstor.org/terms.

[22] J. P. A. Neeft, M. Makkee, and J. A. Moulijn, “Catalytic oxidation of carbon black -1. Activity of catalyst and classification of oxidation profiles”, Fuel 77, 111-119 (1998).

[23] S. Mahamulkar *et al.*, “Formation and Oxidation/Gasification of Carbonaceous Deposits: A Review,” *Industrial and Engineering Chemistry Research*, vol. 55, no. 37. American Chemical Society, pp. 9760–9818, Sep. 21, 2016. doi: 10.1021/acs.iecr.6b02220.

[24] A. Bueno-López, “Diesel soot combustion ceria catalysts,” *Applied Catalysis B: Environmental*, vol. 146, pp. 1–11, Mar. 2014, doi: 10.1016/j.apcatb.2013.02.033.

[25] B. J. Cooper and J. E. Thoss, (1989), “Role of NO in Diesel particulate emission control,” SAE Paper No. 890404, 12 p.

[26] I. Fechete, Y. Wang, and J. C. Védrine, “The past, present and future of heterogeneous catalysis,” in *Catalysis Today*, Jul. 2012, vol. 189, no. 1, pp. 2–27. doi: 10.1016/j.cattod.2012.04.003.

[27] J. N. Armor, “A history of industrial catalysis,” *Catalysis Today*, vol. 163, no. 1, pp. 3–9, Apr. 2011, doi: 10.1016/j.cattod.2009.11.019.

[28] M. Kovacevic, “*Tailored ceria nanoparticles for CO2 mediated ethylbenzene dehydrogenation,”* Doctorate dissertation, University of Twente, (2016).

[29] F. Yang, D. Deng, X. Pan, Q. Fu, and X. Bao, “Understanding nano effects in catalysis,” *National Science Review*, vol. 2, no. 2. Oxford University Press, pp. 183–201, Jun. 01, 2015. doi: 10.1093/nsr/nwv024.

[30] T. Emmerich, “Ceria- and zirconia-based materials for the catalytic oxidation of CO and soot,” Doctorate dissertation, Ruhr-Universität Bochum, (2016).

[31] A. Trovarelli, C. de Leitenburg, M. Boaro, and G. Dolcetti, The utilization of ceria in industrial catalysis, Catal. Today 50 (1999) 353-367.

[32] L. Malavasi, C. A. J. Fisher, and M. S. Islam, “Oxide-ion and proton conducting electrolyte materials for clean energy applications: Structural and mechanistic features,” *Chemical Society Reviews*, vol. 39, no. 11, pp. 4370–4387, Oct. 2010, doi: 10.1039/b915141a.

[33] M. Sim, “Synthesis of Ceria Nanomaterials to Enhance Catalytic Activity of CO Oxidation,” Master’s thesis, Auburn University, Auburn, (2019).

[34] D. Mukherjee and B. M. Reddy, Emiss. Control Sci. Technol. 6, 381 (2020). https://doi.org/10.1007/s40825-020-00170-2.

[35] H. S. Gandhi, A. G. Piken, and M. Shelef, “Laboratory Evaluation of Three-Way Catalysts.”

[36] M. Kovacevic, B. L. Mojet, J. G. van Ommen, and L. Lefferts, “Effects of Morphology of Cerium Oxide Catalysts for Reverse Water Gas Shift Reaction,” *Catalysis Letters*, vol. 146, no. 4, pp. 770–777, Apr. 2016, doi: 10.1007/s10562-016-1697-6.

[37] A. Miri, M. Darroudi, and M. Sarani, “Biosynthesis of cerium oxide nanoparticles and its cytotoxicity survey against colon cancer cell line,” *Applied Organometallic Chemistry*, vol. 34, no. 1, Jan. 2020, doi: 10.1002/aoc.5308.

[38] C. H. Baker, “Harnessing cerium oxide nanoparticles to protect normal tissue from radiation damage,” *Translational Cancer Research*, vol. 2, no. 4, pp. 343–358, Aug. 2013, doi: 10.3978/j.issn.2218-676X.2013.08.15.

[39] Avgouropoulos, G.; Ioannides, T. Selective CO oxidation over CuO-CeO_2 catalysts prepared via the urea-nitrate combustion method. *Appl. Catal. A Gen.*; 2003; *244*, pp. 155-167. [DOI: https://dx.doi.org/10.1016/S0926-860X(02)00558-6].

[40] H. Zhu, Y. Chen, Z. Wang, W. Liu, and L. Wang, “Catalytic oxidation of CO over mesoporous copper-doped ceria catalysts: Via a facile CTAB-assisted synthesis,” *RSC Advances*, vol. 8, no. 27, pp. 14888–14897, 2018, doi: 10.1039/c8ra02327a.

[41] S. Deshpande, S. Patil, S. V. Kuchibhatla, and S. Seal, “Size dependency variation in lattice parameter and valency states in nanocrystalline cerium oxide,” *Applied Physics Letters*, vol. 87, no. 13, pp. 1–3, Sep. 2005, doi: 10.1063/1.2061873.

[42] J. J. A. Flores *et al.*, “Thermal degradation kinetics and FT-IR analysis on the pyrolysis of pinus pseudostrobus, pinus leiophylla and pinus montezumae as forest waste in western Mexico,” *Energies (Basel)*, vol. 13, no. 4, 2020, doi: 10.3390/en13040969.

[43] G. A. Stratakis and A. M. Stamatelos, “Thermogravimetric analysis of soot emitted by a modern diesel engine run on catalyst-doped fuel,” *Combustion and Flame*, vol. 132, no. 1–2, pp. 157–169, Jan. 2003, doi: 10.1016/S0010-2180(02)00432-7.

[44] J. Song, M. Alam, and A. L. Boehman, “Impact of alternative fuels on soot properties and DPF regeneration,” *Combustion Science and Technology*, vol. 179, no. 9, pp. 1991–2037, Sep. 2007, doi: 10.1080/00102200701386099.

[45] D. C. Sau, A. Banerjee, S. Chakravarty, P. Senapti, R. Murmu, and H. Sutar, “Thermal Decomposition Behavior and Kinetic Study of Jamadoba Coal and Its Density Separated Macerals: A Non-Isothermal Approach,” *Advances in Chemical Engineering and Science*, vol. 11, no. 03, pp. 203–227, 2021, doi: 10.4236/aces.2021.113013.

[46] R. Gómez-Hernández, Y. Panecatl-Bernal, and M. Á. Méndez-Rojas, “High yield and simple one-step production of carbon black nanoparticles from waste tires,” *Heliyon*, vol. 5, no. 7, Jul. 2019, doi: 10.1016/j.heliyon. 2019.e02139.

[47] Anthony R. West, “Solid State Chemistry and its Applications, 2nd Edition, Student Edition,” in *Solid State Chemistry*, 2nd ed., vol. 2, London, 2001, pp. 229–265.

[48] Shaw, L. S (n.d.). *Thermal Processing Technology Center Illinois Institute of Technology*. Thermal Processing Technology Center. Retrieved May 20, 2022, from https://sites.google.com/iit.edu/TPTC.

[49] *Pharmaceutical Drug Analysis. Thermoanalytical analysis*. (2018, March 21). Brainkart. Retrieved May 20, 2022, from https://www.brainkart.com/article/Thermogravimetric-Analysis-(TGA)_30856/

[50] A. A. Bunaciu, E. gabriela Udriştioiu, and H. Y. Aboul-Enein, “X-Ray Diffraction: Instrumentation and Applications,” *Critical Reviews in Analytical Chemistry*, vol. 45, no. 4. Taylor and Francis Ltd., pp. 289–299, Oct. 02, 2015. doi: 10.1080/10408347.2014.949616.

[51] S. Nasrazadani and S. Hassani, “Modern analytical techniques in failure analysis of aerospace, chemical, and oil and gas industries,” in *Handbook of Materials Failure Analysis with Case Studies from the Oil and Gas Industry*, Elsevier Inc., 2016, pp. 39–54. doi: 10.1016/B978-0-08-100117-2.00010-8.

[52] M. de Assumpcão Pereira-da-Silva and F. A. Ferri, “Scanning Electron Microscopy,” in *Nanocharacterization Techniques*, 2017. doi: 10.1016/B978-0-323-49778-7.00001-1.

[53] T. Mokkelbost, I. Kaus, T. Grande, and M. A. Einarsrud, “Combustion synthesis and characterization of nanocrystalline CeO 2-based powders,” *Chemistry of Materials*, vol. 16, no. 25, pp. 5489–5494, Dec. 2004, doi: 10.1021/cm048583p.

[54] C. Su, Y. Wang, A. Kumar, and P. J. McGinn, “Simulating real world soot-catalyst contact conditions for lab-scale catalytic soot oxidation studies,” *Catalysts*, vol. 8, no. 6, Jun. 2018, doi: 10.3390/catal8060247.